Available online at www.sciencedirect.com
ScienceDirect
Earth-Science Reviews 79 (2006) 1 – 31
EARTH-SCIENCE REVIEWS
www.elsevier.com/locate/earscirev

How local stresses control magma-chamber ruptures, dyke injections, and eruptions in composite volcanoes

Agust Gudmundsson

Department of Structural Geology and Geodynamics, Geoscience Centre, University of Göttingen, Germany

Received 14 September 2005; accepted 10 June 2006
Available online 28 August 2006

Abstract

To assess the probability of a volcanic eruption during an unrest period, we must understand magma-chamber rupture and dyke propagation to the surface, as well as dyke arrest at depth in the volcano. Dyke propagation and arrest depend strongly on the local stresses in the individual mechanical layers which constitute the volcano. The local stresses are primarily determined by the loading conditions (tectonic stress, magmatic pressure, or displacement) and the mechanical properties of the layers. In the absence of stress monitoring of volcanoes, the local stresses must be inferred from models, either analytical or numerical. This paper reviews many analytical and numerical models of local stresses around magma chambers, as well as analytical models and numerical examples of dyke-injection and eruption frequencies.

Most analytical models of magma chambers ignore the mechanical properties of the individual layers and their contacts, assume the volcano to behave as a homogeneous, isotropic, elastic half space or a semi-infinite plate, and are of two main types: nuclei of strain and cavities. The best-known nucleus of strain is the point-source Mogi model, used to explain surface deformation as a result of either increase or decrease in magma pressure in a chamber whose depth is also inferred from the surface data. The model explains stresses and displacements far away from the chamber, but neither the stress concentration around the chamber, which determines if and where chamber rupture and dyke injection take place, nor the shape, size, and likely tectonic evolution of the chamber.

In the cavity or (two-dimensional) hole model the magma chamber has a finite size. Thus, the local stresses at, and away from, the boundary of a chamber can be calculated. For various loading conditions, an analytical cavity model gives a crude indication of the local stresses in a volcano and its surface deformation. However, variation in mechanical properties, and contacts, between layers are ignored. The analytical cavity model thus cannot be used for detailed analyses of the local stresses in a composite volcano.

The numerical models presented here show that the local stresses in a volcano depend strongly on the magma-chamber geometry and the mechanical properties of its layers which are often contrasting, particularly at shallow depths. For example, lava flows, welded pyrolastic units, and intrusions may be very stiff (with a high Young's modulus), whereas young and non-welded pyroclastic and sedimentary units may be very soft (with a low Young's modulus). Consequently, the local stresses may change abruptly from one layer to the next; for example, one layer may favour dyke propagation while an adjacent layer favours dyke arrest. No dyke-fed eruption can occur if there is any layer along the potential path of the dyke to the surface where the stress field is unfavourable to dyke propagation. If such a layer occurs, the dyke normally becomes arrested and an eruption is prevented. The present results indicate that during unrest periods composite volcanoes commonly develop local stresses that arrest dykes and prevent eruptions, in agreement with field observations. These results underline the need for in situ stress monitoring of volcanoes to assess the probability of dyke-fed eruptions.

Keywords: volcanic eruption; dyke injection; magma chamber; crustal stress; layered crust; volcanotectonic modelling

E-mail address: Agust.Gudmundsson@gwdg.de.

0012-8252/$ - see front matter © 2006 Elsevier B.V. All rights reserved.
doi:10.1016/j.earscirev.2006.06.006

1. Introduction

In recent decades, there has been considerable progress in the general understanding of the hazards involved once an eruption has started. The improved understanding applies, in particular, to the dynamics of eruptive columns (Sparks et al., 1997) and the formation and mechanics of transport of pyroclastic rocks (Fisher and Schmincke, 1984; Cas and Wright, 1987; Freundt and Rosi, 2001; Schmincke, 2004). But there has also been considerable advancement in the general knowledge of the evolution of basaltic lava flow fields such as those that occur worldwide at the surfaces of mantle plumes and other basaltic provinces (Walker, 1991; Kilburn and Lopes, 1991; Self et al., 1996; Rossi, 1996; Calvari et al., 2003).

Most volcanic unrest periods, however, do not result in an eruption (Newhall and Dzurisin, 1988). Even those unrest periods where magma-driven fractures (dykes or inclined sheets) are known to be injected from a shallow magma chamber do not normally result in an eruption (Pollard et al., 1983; Lister and Kerr, 1991; Rubin, 1995; Bonafede and Rivalta, 1999; Pinel and Jaupart, 2000; Gudmundsson, 2002, 2003; Acocella and Neri, 2003; Stewart et al., 2003, 2005; Rivalta et al., 2005).

Since nearly all volcanic eruptions are supplied with magma through dykes and inclined sheets, it follows that for an eruption to occur a dyke or a sheet must be able to propagate from a magma chamber to the surface. The initiation of a dyke and its eventual propagation to the surface or, alternatively, arrest at some depth in the volcano, depend on the state of stress in the volcano. This stress state is controlled, first, by the mechanical properties of the rocks that constitute the volcano and the associated crustal segment and, second, by the shape, depth, and loading conditions of the source magma chamber or chambers. In solid mechanics, "load" is a word that normally means the forces, stresses, or pressures applied to a body and external to its material (Benham et al., 1996). Accordingly, in this paper "loading conditions" refer to the stresses and magmatic pressures applied to the magma chambers in the analytical and numerical models.

To understand and assess the hazard during an unrest period, we must know the state of stress in the volcano and, in particular, the stress concentration around the magma chamber or chambers that supply magma to its eruptions. Mechanically, partly or completely solidified magma chambers (plutons) that have properties different from those of the host rock are analogous to inclusions in an elastic body; completely molten chambers are analogous to cavities. In two-dimensional models, cavities are referred to as holes. All cavities and inclusions in an elastic body disturb the stress field of that body and give rise to stress concentrations (Fig. 1).

Stress concentrations around magma chambers are responsible for their ruptures and dyke or sheet injections during periods of unrest. As a result of stress concentration, a local stress field develops around the chamber and in its vicinity. This local field determines whether an injected sheet intrusion becomes a sill, an inclined sheet, or a subvertical dyke (Fig. 2). In this paper the word "dyke" is used mostly as a generic term, covering both proper dykes and inclined sheets. When necessary, however, a distinction is made between subvertical dykes and inclined sheets. Also, when discussing results applicable to composite volcanoes it is implied that the same results may apply to composite rift zones.

To understand the mechanics of a composite volcano (central volcano, stratovolcano) one must know the stress fields associated with its source magma chamber. Some authors have modelled the host rock of the chamber as viscoelastic (Bonafede et al., 1986; Folch et al., 2000). Here, however, the focus is on host-rock behaviour that can be described to a first approximation as elastic. When the rock hosting the chamber is

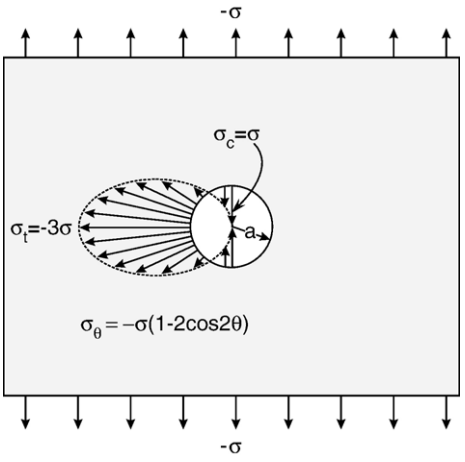

Fig. 1. Any hole or cavity in a solid material subject to loading gives rise to stress concentration. The same applies to inclusions with material properties different from those of the hosting solid material (the matrix). For a circular hole subject to tensile stress $-\sigma$ the stress at its boundary is given by the equation $\sigma_\theta = -\sigma(1-2\cos 2\theta)$ where the maximum tensile stress at its boundary is $\sigma_t = -3\sigma$ (cf. Eq. (16) with $b=c$) and occurs at the transverse diameter ($\theta = \pm 90°$). For the longitudinal diameter ($\theta = 0°$, 180°) there is compressive stress of magnitude $\sigma_c = \sigma$. Mechanically, fluid magma chambers are analogous to holes (two-dimensional models) or cavities (three-dimensional models), whereas partially molten chambers are analogous to inclusions (modified from Boresi and Sidebottom, 1985).

modelled as homogeneous (with the same properties everywhere) and isotropic (with properties independent of direction of measurement), analytical solutions exist for the local stress field (e.g., Gudmundsson, 1988; Pinel and Jaupart, 2003). Some of these solutions are reviewed below. Generally, however, the rock hosting the chamber is heterogeneous and anisotropic. There exist some analytical solutions for magma chambers (holes, cavities) in anisotropic bodies (Savin, 1961; Lekhnitskii, 1968; Tan, 1994), as well as for very simple aspects of micromechanical (micropolar) theories (Sadd, 2005). However, because of the complexity of the overall properties of heterogeneous, elastic materials (Nemat-Nasser and Hori, 1999), simple, closed-form analytical stress solutions such as can be applied to magma chambers in heterogeneous and anisotropic crustal segments are generally not available. It follows that the stress fields around magma chambers in anisotropic and heterogeneous crustal segments must normally be obtained using numerical models. Many numerical models of stress fields around magma chambers are given below.

It should be emphasised that although most of the field and numerical examples are from Iceland, the results presented here are applicable to any composite volcano. This follows because the condition for magma-chamber rupture and dyke injection (Eq. (1)) is universal and does not depend on the tectonic regime within which the volcano is located. Also, in the numerical models the magma-chamber shapes or the mechanical properties of the layers, of course, do not depend on the associated tectonic regime. Furthermore, even if the loading conditions used in the models may be reached in different ways in different tectonic regimes, the calculated stresses depend only on the loading conditions used and not on how they were reached. For example, if the conditions for dyke injection (Eq. (1)) are reached through reduction in the minimum compressive principal stress σ_3, it does not matter if that reduction is reached through divergent plate movements (at an ocean ridge), doming (in a continental region), or extension in a transtension region associated with a major strike-slip fault.

Most of the field examples are from composite volcanoes in Iceland; these are traditionally referred to as central volcanoes (Walker, 1963; Saemundsson, 1978; Gudmundsson, 2000). Some are stratovolcanoes that rise high above their surroundings, others are calderas (Fig. 3). Inside the rift zone, the volcanoes tend to be located near the centre of the associated volcanic system, and erupt much more frequently than the rest of the system, hence the name central volcano. Because of this tradition, in this paper the terms "central volcano" and "volcano" are commonly used for the composite volcanoes and calderas of Iceland.

The general emphasis, however, is on the terms "composite volcano" and "composite rift zone" for two main reasons. First, all volcanoes and rift zones are composite in that they consist of layers with (often widely) different mechanical properties (Fig. 4). Also, some layers may be regarded as located in a "matrix" or units of very different mechanical properties. Second, the mechanical behaviour and local stresses of composite volcanoes are formally similar to those of general composite materials (Daniel and Ishai, 1994; Tan, 1994; Kaw, 1997; Hyer, 1998). By emphasising this similarity, local stresses in volcanoes can be compared with, and understood in terms of, general results on stress variations in composite materials.

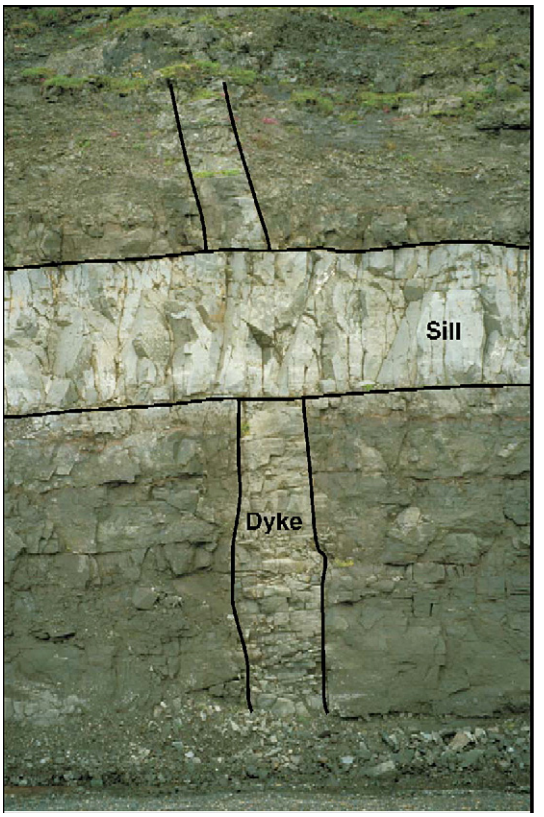

Fig. 2. Cross-cutting relation between a subvertical basaltic dyke and a subhorizontal sill in the Tertiary lava pile in Southeast Iceland. View northeast, the sill is about 2 m thick, the dyke about 1 m. There is no sheet-parallel displacement where the intrusions cross cut, indicating that the younger intrusion (the sill) is a pure extension (mode I) fracture. Similar results are obtained worldwide suggesting that most sills, dykes, and inclined sheets are extension fractures. Inclined sheets dip between the extremes of a dyke and a sill (Fig. 25; cf. Fig. 6 in Gudmundsson, 2002).

Many, perhaps most, composite volcanoes are supplied with magma from shallow magma chambers which, in turn, receive their magmas from deeper reservoirs. Such a pair is referred to as a double magma chamber (Fig. 5). Commonly, the deep-seated chamber or reservoir is much larger than the shallow chamber and located in the lower crust or at the crust-mantle boundary (Gudmundsson, 2000). A single magma flow from the deeper reservoir may then trigger many dyke injections, and eventually eruptions, from the shallow chamber. It follows that the deeper reservoir has great effects on the rupture frequency of the shallow chamber and, indirectly, on the eruption frequency of the associated volcano.

This paper has three main aims. The first aim is to review existing analytical and numerical models on the local stresses that develop in major composite volcanoes and rift zones supplied with magma from shallow chambers and deeper reservoirs. To make the treatment completely up-to-date, I also discuss the results of several new numerical models. Three basic models are considered. First, single and double magma chambers in a homogeneous, isotropic crustal segment. For this case both analytical and numerical models are presented. Second, numerical models of the stress fields around single magma chambers in a layered crustal segment. And, third, numerical models of the stress fields around double magma chambers in a layered crustal segment.

The second aim is to review existing, and present some new, results on the conditions of magma-chamber rupture and dyke injection. Particular attention is given to the effects that abrupt changes in local stress fields have on the propagation and arrest of dykes. Also, simple stress analysis is used to explain the typical

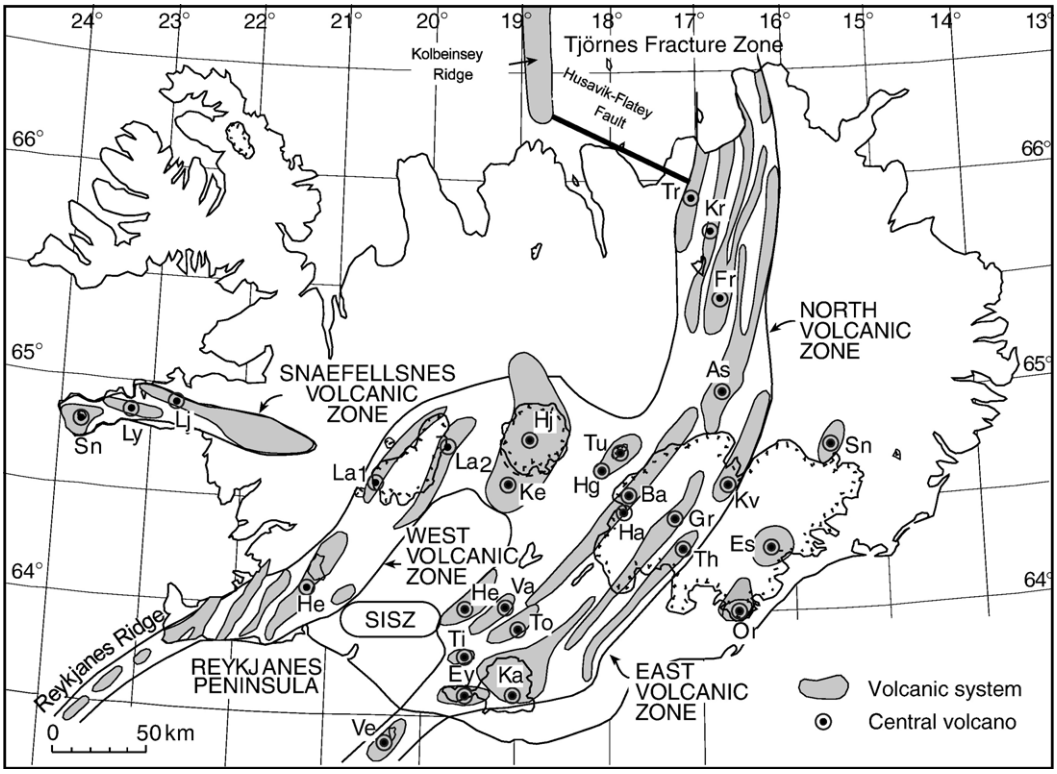

Fig. 3. Active volcanic systems, composite volcanoes, and calderas in Iceland. Most of the composite volcanoes indicated by abbreviated names have collapse calderas. The named volcanic systems are: Tr=Theystareykir, Kr=Krafla, Fr=Fremri–Namur, As=Askja, Kv=Kverkfjöll, Th=Thordarhyrna, Gr=Grimsvötn, Ha=Hamarinn, Ba=Bardarbunga, Tu=Tungnafellsjökull, Hg=Hagöngur, Ka=Katla, Ey=Eyjafjallajökull, Ve=Vestmannaeyjar, Ti=Tindfjallajökull, Va=Vatnafjöll, He=Hekla, Hj=Hofsjökull, Ke=Kerlingafjöll, La1&2=Langjökull, He=Hengill. The other systems on the Reykjanes Peninsula (from east to west) are Brennisteinsfjöll, Trölladyngja and Reykjanes. Off-coast are Eldey, Geirfuglasker and Eldeyjarbodi. In the Snaefellsnes Volcanic Zone are the systems Sn=Snaefellsjökull, Ly=Lysuskard, and Lj=Ljosufjöll. Outside the East Volcanic Zone are the systems Or=Oraefajökull, Es=Esjufjöll, and Sn=Snaefell. The rift zone comprises the North Volcanic Zone, the West Volcanic Zone, and the East Volcanic Zone to the south tips of the volcanic systems of Bardarbunga and Grimsvötn. The main ocean-ridge discontinuities are also indicated: the Husavik–Flatey Fault of the Tjörnes Fracture Zone and the South Iceland Seismic Zone (SISZ), located between the overlapping West and East Volcanic Zones. Modified from Gudmundsson (2000).

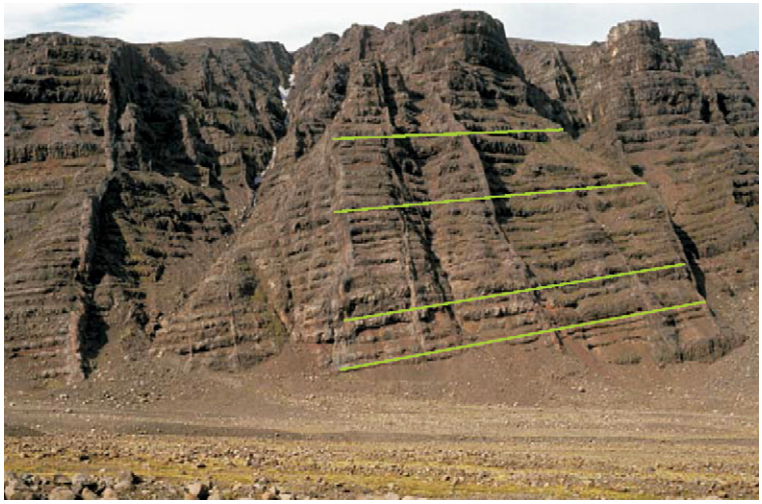

Fig. 4. Layered, Tertiary palaeorift zone in Southeast Iceland eroded and exposed to a depth of nearly 2 km beneath the original surface. View northeast, the green, thin lines indicate how the dip of the lava flows and pyroclastic layers in the 400-m-thick pile increases with depth by some 2–3°. A regional swarm of subvertical, basaltic dykes cuts through the pile. Many dykes are offset, and some arrested, at layer contacts. Cf. Figs. 29 and 30.

injection frequencies of dykes associated with single and double magma chambers.

The third aim is to review and extend the current knowledge of the conditions for dykes reaching the surface in composite volcanoes and rift zones, that is, the conditions for dyke-fed volcanic eruptions. The main attention is given to the effects of mechanical layering in composite volcanoes and rift zones on the local stress fields, and how these largely determine whether an injected dyke is able to reach the surface and supply magma to an eruption.

In Section 8 of the paper, some of the main theoretical results are used to quantify the stress conditions for magma-chamber rupture and the frequency of dyke injections for certain specified boundary conditions.

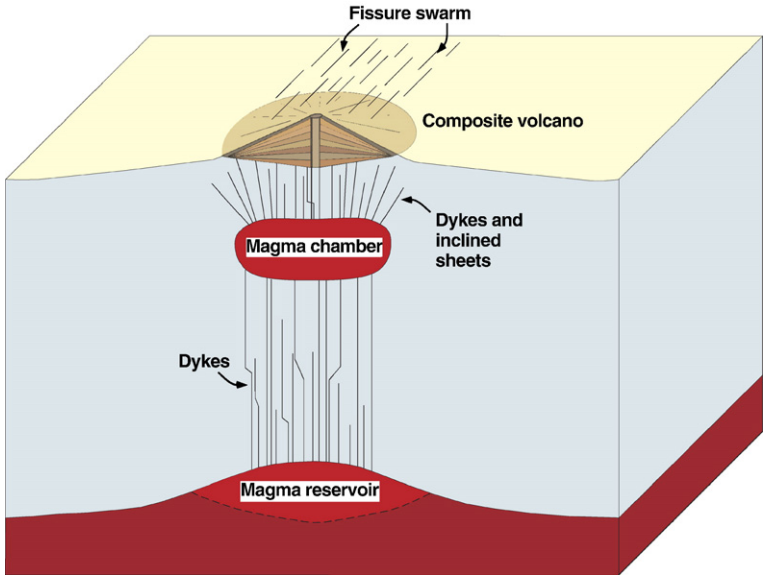

Fig. 5. Schematic illustration of a double magma chamber supplying magma to a composite volcano and the associated volcanic system, the surface expression of which is a fissure swarm. The deep-seated magma reservoir is elongate, underlies a large part of the volcanic system, and is much larger than the shallow magma chamber beneath the composite volcano itself. The composite volcano is composed of layers that, at the surface, are outward-dipping but gradually become inward-dipping at greater depth.

2. The two basic models

The most commonly used models of a magma chamber are of two basic types. One type regards the magma chamber simply as a pressure source in an elastic crustal segment, commonly a point source, without any finite-size geometry. This model is primarily used to explain surface deformation as obtained from geodetic measurements during periods of unrest. The other basic type regards the magma chamber as a finite-size body in an elastic crustal segment: a hole for two-dimensional models, and a cavity for three-dimensional models. Both basic models can be presented through analytical solutions, in which case the elastic crustal segment is normally regarded as homogeneous and isotropic. For realistic modelling of stress fields and surface deformation associated with a composite volcano, however, the crustal segment hosting the chamber must be regarded as heterogeneous and, in particular, as layered. For such host rocks, numerical models are normally used.

2.1. Nucleii of strain

During periods of unrest in a volcano its surface deformation is traditionally explained in terms of a pressure change in the associated magma chamber modelled as a nucleus of strain. This is the so-called "Mogi model", a widely used model in volcanology (Mogi, 1958). In this model, the chamber is regarded as a concentrated (point) force of an infinitesimal volume (Fig. 6). The stresses and displacement produced by a nucleus of strain located at a certain distance below the surface of a semi-infinite elastic body or an elastic half space can be obtained through analytical solutions. These solutions were initially derived by Melan (1932) and Mindlin (1936) and used in geology by Anderson (1936).

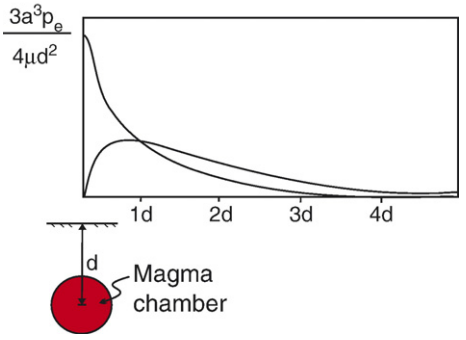

Fig. 6. Mogi (point-source) model, an analytical model commonly used to explain the surface deformation during unrest periods in composite volcanoes. The vertical displacement of the surface, maximum above the chamber, is indicated by the upper curve whereas the horizontal displacement is indicated by the lower curve. The chamber, with a radius a, is subject to excess magma pressure p_e (Eq. (1)); its centre is located at depth d below the surface (cf. Fig. 11). The host rock has a shear modulus μ; for a rock with a typical Poisson's ratio of 0.25, Young's modulus $E=2.5\mu$.

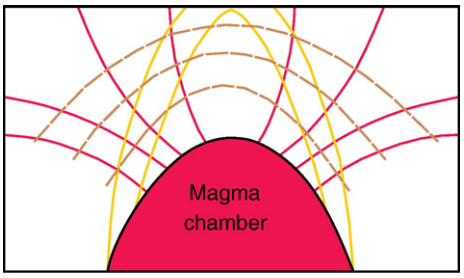

Fig. 7. Nuclei-of-strain model for the formation of inclined (cone) sheets and ring dykes (Anderson, 1936). When the pressure in a chamber exceeds the lithostatic pressure (by an excess pressure p_e), modelled by Anderson as an upward point push, the broken brown lines represent the trajectories of σ_3 and the orthogonal solid red lines the trajectories of σ_1. Inclines sheets would propagate along the σ_1-trajectories. When the pressure in the chamber decreases below lithostatic pressure (an underpressure or negative excess pressure), modelled by Anderson as a downward point push, a ring dyke is supposed to be injected between the solid, subvertical yellow lines.

Using nuclei of strain, Anderson (1936) was able to explain, in formal terms, the trends of dykes and inclined sheets injected from a magma chamber located in a homogeneous, isotropic elastic half space. Since dykes and sheets are mostly extension fractures they follow the trends (trajectories) of the maximum principal compressive stress, σ_1, and are perpendicular to the minimum compressive, maximum tensile, principal stress, σ_3 (Gudmundsson, 2002). From his nucleus-of-strain model, Anderson (1936) calculated the orientations of the principal stresses and, thereby, the trends of ideal dykes and inclined sheets far away from the magma chamber (the strain nucleus) itself (Fig. 7). Using a nucleus of strain referred to as centre of compression (Love, 1927) for a magma chamber, Anderson (1936) also presented a model of collapse-caldera formation as being the result of magma-chamber underpressure, that is, compression or contraction of an associated magma chamber.

For half a century, nuclei of strain have been routinely used to account for surface deformation in volcanoes (Mogi, 1958; Bonafede et al., 1986; Davis, 1986; McTigue, 1987; Delaney and McTigue, 1994; Battaglia et al., 2003). Most of these models assume that the stresses and displacements generated by the nucleus correspond to be those produced by an excess magmatic pressure – or, for collapse calderas in Anderson's (1936) model, magmatic underpressure – in a spherical chamber associated with the volcano (Figs. 6 and 7). Another

common model assumption is that the magma chamber is located at comparatively great crustal depths. This implies that the chamber depth below the surface of the composite volcano is large in comparison with the chamber diameter.

Displacements generated by nuclei of strain can often be fitted to the observed surface deformation during a period of volcanic unrest (Fig. 6). Inversion of the surface data may then give a crude indication of the depth to the pressure change associated with that particular unrest period. It is normally assumed that the point pressure or pressure change occurs somewhere near the top of an associated magma chamber. Sometimes the pressure change does indeed occur near the top of a chamber, but during many unrest periods that assumption is not warranted. For example, the apparent pressure change may be primarily associated with stress concentrations and, eventually, sheet injections from the margins of the chamber. Also, faulting and various other tectonic and thermal processes may cause surface deformation during unrest periods. Interpreting these as pressure changes near the top of a magma chamber may result in a mistaken picture of the physical processes responsible for the surface deformation. For these reasons, the physical meaning of models which use nuclei of strain to interpret surface deformation of volcanoes is commonly obscure.

There are also other reasons why nuclei of strain must be regarded as unsatisfactory models of magma chambers. One is that a nucleus-of-strain model does not make it possible to draw any further conclusions regarding the infrastructure or tectonic evolution of the composite

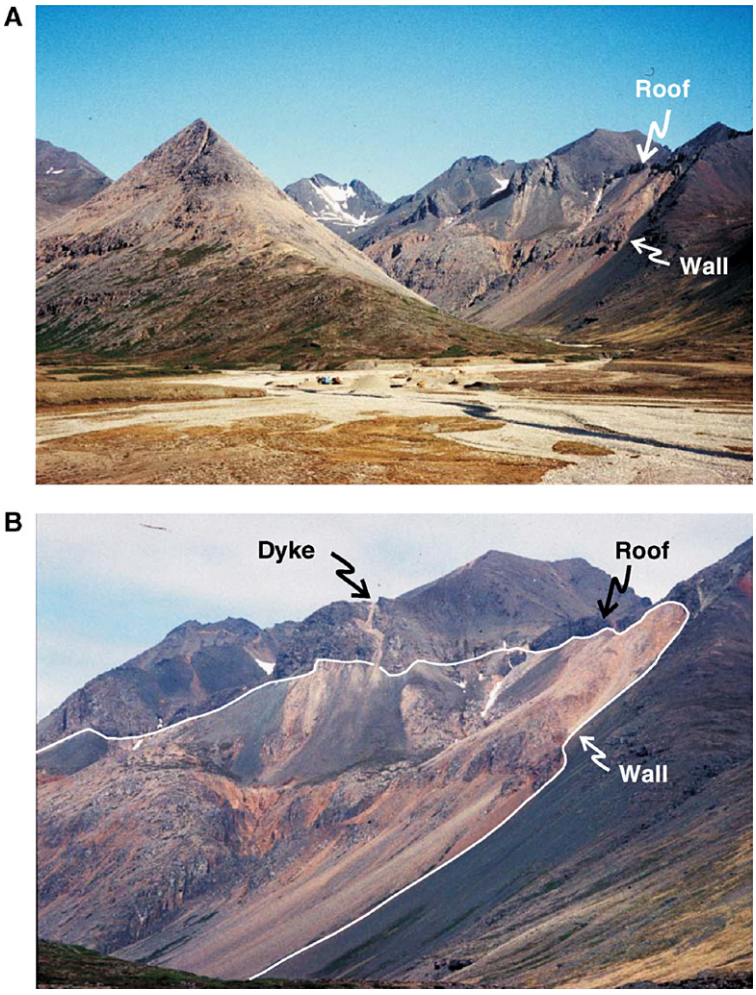

Fig. 8. Slaufrudalur pluton in Southeast Iceland (cf. Fig. 9). A) The pluton is the uppermost part of an extinct, shallow magma chamber with an exposed area of 15 km^2 and volume, all of which is made of granophyre, of about 10 km^3 (Cargill et al., 1928; Beswick, 1965). The pluton age is between 6.5 and 10 Ma (Torfason, 1979). B) Parts of the roof and the walls (outlined) of the pluton are exceptionally well exposed. The roof is dissected by many acid dykes (one is indicated), demonstrating that the pluton acted as a chamber. There are also basaltic sheets cutting the pluton.

volcano that is undergoing unrest. A particular nucleus-of-strain model can normally be fitted to the surface deformation of a volcano only during a certain short unrest period. Such a model considers neither the effects of a real, finite-size magma chamber nor the tectonic evolution of the chamber and the associated volcano. It follows that a nucleus-of-strain model tells us next to nothing about the real volcanotectonic processes associated with the unrest. There are fundamental questions that arise during each unrest period, such as: Is the volcano likely to erupt, and if so where? Alternatively, is the volcano likely to develop a collapse caldera or generate a landslide? A nucleus-of-strain model of the magma chamber does not help answering these and related questions.

A second reason is that the nucleus-of-strain model can in principle only account for the displacement and stresses far away from the chamber, but not those that occur in the vicinity or at the margin of the chamber. This limitation is because the nucleus-of-strain model substitutes actual magma chambers with vanishingly small point sources. Thus, the magnitude and location of the maximum stress concentration around the chamber itself – factors that determine if and where chamber rupture and magma injection takes place during an unrest period – cannot be determined when the chamber is modelled as a nucleus of strain.

Part of many extinct magma chambers are currently exposed as plutons with volumes of 1–10 km^3 although some are much larger (Sibett, 1988; Marsh, 1989). Similarly, active magma chambers are widely considered to have volumes ranging from less than 5 km^3 to about 500 km^3 (Chester, 1993). A corresponding, active spherical chamber would have a radius from less than 1 km to about 5 km. Magma chambers associated with active composite volcanoes are thus likely to be of considerable volumes. Many shallow chambers are also large in comparison with their depths below the surfaces of the volcanoes. Magma chambers, particularly shallow ones, are thus likely to develop local stress and displacement fields for which nucleus-of-strain models are not appropriate.

2.2. Cavities

The considerations above indicate that all shallow magma chambers are of finite, and often considerable, sizes. Most chambers, particularly shallow ones, are located in crustal segments that, during most unrest periods, behave as elastic. It follows that an appropriate mechanical model of a typical magma-filled chamber is a finite-size cavity or, for a two-dimensional model, a hole in an elastic plate or half space. Many magma chambers, however, are presumably partially molten,

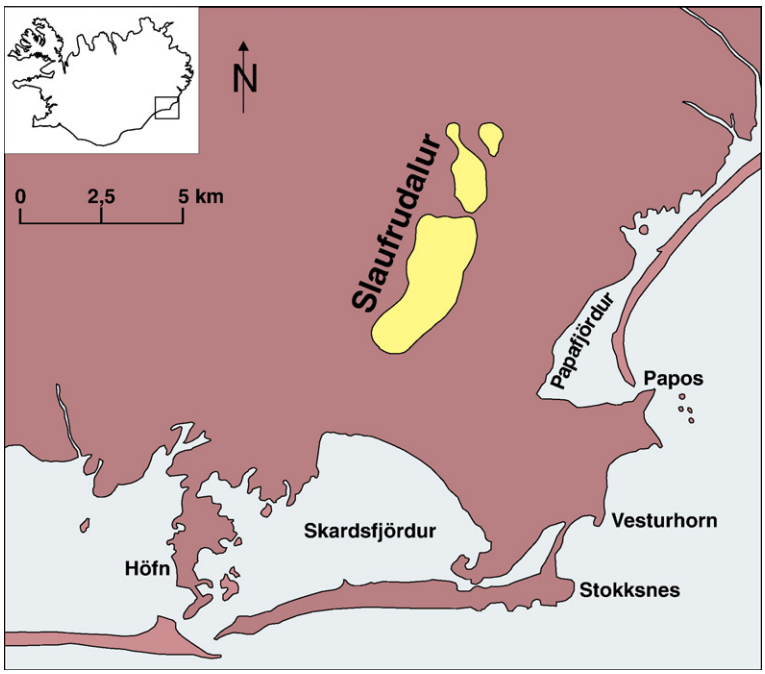

Fig. 9. Simplified geological map of the Slaufrudalur pluton (an extinct shallow magma chamber) in Southeast Iceland (data from Cargill et al., 1928; Beswick, 1965). The pluton is elongate in the direction of the palaeorift zone, about 8 km long and with a maximum width of 2 km (cf. Fig. 8).

that is, composed partly of magma and partly of a crystal mush. In that case, a chamber may be regarded as an inclusion (Goodier, 1933; Eshelby, 1957; Savin, 1961) the stiffness (Young's modulus) of which increases as the magma fraction decreases.

When using a cavity model, the magma chamber can have any size or depth below the surface of its volcano. The chamber may also be subject to any type of loading, such as internal excess magmatic pressure (Bonafede et al., 1986; Folch and Marti, 1998; Gudmundsson, 1998; Folch et al., 2000), external stresses, or external displacements (Savin, 1961; Gudmundsson, 1988, 2002). For a cavity model, it is possible to calculate the stress concentration around the chamber, and thus to identify the potential regions of rupture and dyke injection. Furthermore, the trajectories of the principal stresses in the vicinity of the cavity chamber determine the propagation directions of ideal dykes injected from the chamber.

Three-dimensional cavity models and two-dimensional hole models of magma chambers can also easily be analysed using numerical programs. In such models the magma chamber may have any shape, and heterogeneities can be added to the crustal segment hosting the chamber: for example, layers with contrasting mechanical properties, such as soft pyroclastic layers alternating with stiff lava flows, as are common in many composite volcanoes (Gudmundsson, 2002; Gudmundsson and Brenner, 2004a, b, 2005; Trasatti et al., 2005). Numerical programs make it possible to calculate the stress trajectories for any kind of loading, volcano geometry, magma-chamber geometry, host-rock layering, anisotropy, and dyke–dyke or dyke–fault interactions (De Natale and Pingue, 1993; Gudmundsson and Brenner, 2004a,b, 2005; Lungarini et al., 2005; Trasatti et al., 2005). It follows that numerical cavity models can be used to explain, in formal terms, the attitude of all sheets and dykes injected from magma chambers.

Many near-surface solid rocks are at low temperature and pressure and behave as elastic up to strains of about 1% (Farmer, 1983). Expansion of a cavity-like magma-chamber prior to rupture and dyke injection would

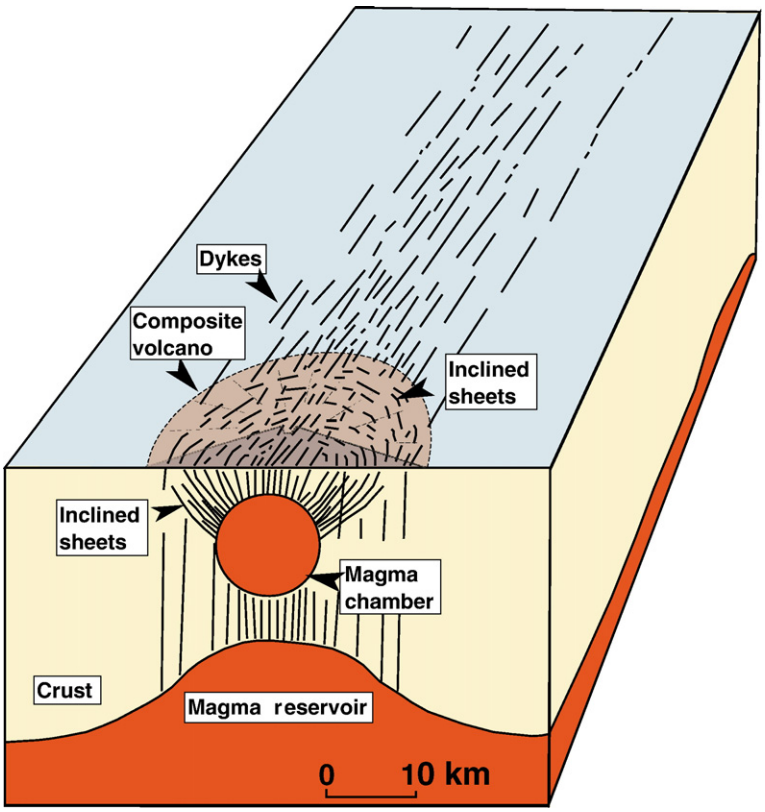

Fig. 10. At divergent plate boundaries, elongate magma reservoirs normally underlie large parts of the volcanic rift zones. In Iceland, for example, reservoirs supply magma directly to many shield volcanoes and fissure eruptions in the parts of the volcanic systems outside the associated composite volcanoes (Gudmundsson, 2000). In inactive and partly eroded volcanic systems, the composite volcano (here half of the former volcano, shown in brown, is outlined) is characterised by a dense swarm of thin inclined sheets and, when deeply eroded, plutons (uppermost part of an extinct magma chamber) in its core (cf. Fig. 25). The parts outside the composite volcano are characterised by a swarm of subvertical, thick regional dykes (cf. Fig. 4).

rarely generate host-rock strains exceeding this limit. At the depths of most active magma chambers, however, rocks are subject to pressure and temperature much higher than near the surface. Increasing temperature generally lowers the stiffness of the rock hosting the chamber (Hudson and Harrison, 1997; Schön, 2004). By contrast, the stiffness tends to increase with crustal depth partly as a result of healing and sealing of contacts and filling of pores with secondary minerals. The temperature and depth effects on host-rock stiffnesses can be taken into account by altering the effective Young's modulus of the rock. Reasonably realistic cavity models of magma chambers can normally be provided on the assumption that the rock behaves as linear elastic. That assumption is used in the following sections.

3. Stress concentrations around chambers

The simplest finite-size model of a magma chamber is a circular hole. In physical terms, this is a two-dimensional model which is suitable when one of the magma-chamber dimensions is very large in comparison with the other two. For example, the chamber may be elongate parallel with the axis of the rift zone within which it is located. This is so for some extinct shallow magma chambers in Iceland, for example the Slaufrudalur pluton (Figs. 8 and 9). Elliptical calderas indicate that elongate shallow magma chambers may be quite common (Acocella et al., 2003; Holohan et al., 2005).

There are also indications that many deep-seated magma chambers underlying large parts of the rift-zone volcanic systems are elongate parallel to the volcanic systems (Fig. 10). For a chamber where one horizontal dimension of is much larger than the other two dimensions, the large dimension may often be assumed infinite, in which case the stress-concentration problem is reduced to two dimensions. Many chambers, however, may be approximately spherical, in which case a three-dimensional model is more appropriate.

Stress concentration around a chamber decides whether it ruptures. A magma-chamber ruptures and initiates a dyke when the following equation is satisfied (Gudmundsson, 1990):

$$p_l + p_e = \sigma_3 + T_0 \quad (1)$$

Here, p_l is the lithostatic stress or overburden pressure at the rupture site; $p_e = P_t - p_l$ is the difference between the total magma pressure P_t in the chamber at the time of its rupture and the lithostatic stress, and is referred to as excess pressure — also referred to as overpressure (Bonafede et al., 1986; Folch and Marti, 1998; Folch et al., 2000; Pinel and Jaupart, 2003); σ_3 is the minimum compressive or maximum tensile principal stress, and T_0 the local in situ tensile strength, at the rupture site. Following the tradition in geology, compressive stress is considered positive. Thus, for an absolute tension to occur, σ_3 must be negative. By contrast, the maximum compressive principal stress σ_1 is always positive. In subsequent sections of this paper, when σ_3 has no sign, it is understood to be the absolute value of the maximum tensile principal stress, that is, $|\sigma_3|$.

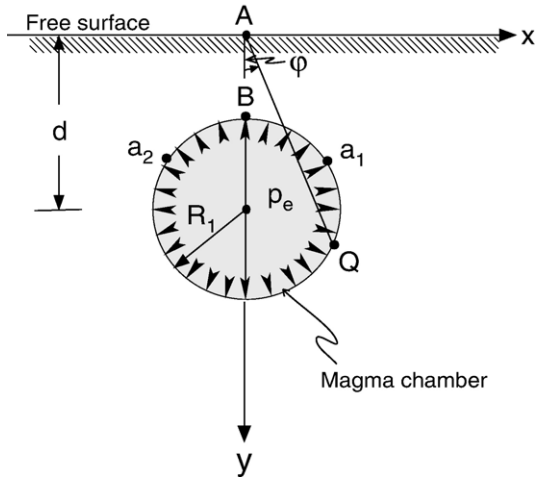

Fig. 11. Shallow, circular magma chamber of radius R_1, its centre being at depth d below the free surface, is subject to excess magma pressure p_e. The line AQ is tangent to the boundary of the chamber at points a_1 and a_2. There the angle φ is maximum and the tensile stresses at the boundary of the chamber peak. On the boundary of the chamber, point B is the one next to the free surface where its projection is point A.

3.1. Holes subject to internal pressure

Consider a two-dimensional magma chamber modelled as a hole with a circular vertical cross section of radius R_1 and depth to centre d (Fig. 11). The chamber is subject to excess magmatic pressure p_e as the only loading (Eq. (1)). The stress σ_x at the surface of the associated composite volcano or a rift zone is then given by (Jeffrey, 1921; Savin, 1961):

$$\sigma_x = 4p_e\left[\frac{R_1^2(x^2 - d^2 + R_1^2)}{(x^2 + d^2 - R_1^2)^2}\right] \quad (2)$$

The maximum tensile stress σ_t at the surface of the volcano occurs at point A (with $x = 0$; Fig. 11), and its magnitude is:

$$\sigma_t = -\frac{4p_e R_1^2}{d^2 - R_1^2} \quad (3)$$

The stress σ_t may generate tension fractures at the surface of the associated composite volcano during magma-chamber inflation, that is, increased magmatic pressure. At the points $x=|(d^2-R_1^2)^{1/2}|$, however, σ_t becomes compressive. Its largest compressive value, σ_c, occurs at points $x=|3(d^2-R_1^2)^{1/2}|$ and has a magnitude of:

$$\sigma_c = \frac{p_e R_1^2}{2(d^2-R_1^2)} \quad (4)$$

The absolute value of σ_c is equal to 1/8 of that of σ_t.

The rupture and dyke injection normally occur where, at the boundary of the chamber, the tensile stress concentration during a particular unrest period reaches a maximum. The tangential or circumferential stress at the boundary of the chamber σ_θ is:

$$\sigma_\theta = -p_e(1+2\tan^2\phi) \quad (5)$$

where the angle ϕ is defined in Fig. 11. Normally, it is the upper part of the chamber that ruptures, so I focus on that part here. From Eq. (5) it follows that the peak value of σ_θ, denoted by σ_b, occurs where the angle ϕ is maximum, namely at the points a_1 and a_2 where the line AQ is tangent to the boundary of the magma chamber (Fig. 11). At these points, the maximum tensile stress reaches the value:

$$\sigma_b = -\frac{p_e(d^2+R_1^2)}{d^2-R_1^2} \quad (6)$$

From Eqs. (5) and (6), we can conclude as follows:

- If $d>1.73R_1$, the maximum tensile stress associated with the chamber occurs at its boundary, at points a_1 and a_2 (Fig. 11), and is given by Eq. (6). This stress field favours dyke injection.
- If $d<1.73R_1$, the maximum tensile stress associated with the chamber occurs not at its boundary but rather at the surface of the associated composite volcano, at point A (Fig. 11), and is given by Eq. (3). This stress field favours the formation of tension fractures at the surface and is unlikely to trigger dyke injection.
- If $d=1.73R_1$, the maximum tensile stresses at the surface of the composite volcano is equal to that at the boundary of the chamber, with a magnitude of $\sigma_b=\sigma_t=2p_e$.

At point B (Fig. 11) the tensile stress is equal to p_e, whereas at points A, a_1 and a_2 the tensile stress always exceeds p_e. At points A, a_1 and a_2 the stress depends on the difference between the depth to the centre of the chamber d and the chamber radius R_1. Since Eqs. (3) and (6) both have $d^2-R_1^2$ in the denominator, then when $R_1\rightarrow d$, that is, when the depth to the top (point B) of the chamber decreases, σ_b and σ_t can, theoretically, become many times greater than p_e. In nature, however, the tensile stress at the boundary of the chamber is limited by the local tensile strength of the host rock, normally 0.5–6 MPa (Haimson and Rummel, 1982; Schultz, 1995). When the condition of Eq. (1) is reached at points a_1 and a_2, there will be sheet or dyke injection that immediately relaxes the tensile stress at the boundary of the chamber. Since most chambers are at considerable depths in comparison with their radii, d would rarely be very similar to R_1. Also, tensile stress concentration around real three-dimensional chambers (cavities) would normally be less than that indicated by these two-dimensional (hole) results.

3.2. Cavities subject to internal pressure

An ideal three-dimensional magma chamber is an ellipsoidal cavity (Gudmundsson, 1988) with the shape of a sphere, an oblate ellipsoid, or a prolate ellipsoidal (Sadowsky and Sternberg, 1947, 1949; Tsuchida and Nakahara, 1970; Soutas-Little, 1973). For a spherical magma chamber comparatively close to the surface of the associated composite volcano, that is, for a cavity in an elastic half space (with a free top surface), analytical closed-form solutions have been obtained by Keer et al. (1998). Similarly, Tsuchida and Nakahara (1970) provide analytical solutions for a cavity in a semi-infinite plate (with free surfaces at its top and bottom) and elastic half spaces. These solutions are too complex to be given here.

For magma chambers at depths that are great in relation to their sizes there exist simple analytical solutions for the stress fields. If the chamber radius R_1 is much smaller than the distance d to its centre from the free surface of the composite volcano, then the stresses at the chamber boundary and beyond can be calculated form the well-known equations for a hollow sphere under internal pressure. In this model, the chamber is subject to a total magmatic pressure $P_t=p_e+p_l$ as the only loading (Eq. (1)). The chamber radius is R_1 and the margin of the elastic crust hosting the chamber is also assumed to be a sphere with a radius R_2. When compared with R_1 then R_2 is effectively infinite, so that $R_2 \gg R_1$, and there is lithostatic stress p_l at R_2.

For this analysis, we use spherical polar coordinates (r,θ,ϕ), where r is the radius vector (distance), θ is the angle between the radius vector r and a fixed axis z, and ϕ is the angle measured around this axis (Fig. 12). The radial stress σ_r away from the chamber and due to the chamber excess pressure is then (Saada, 1983; Gudmundsson, 2002):

$$\sigma_r = P_t\left(\frac{R_1}{r}\right)^3 + p_l\left[1-\left(\frac{R_1}{r}\right)^3\right] \quad (7)$$

Spherical symmetry implies that the two other principal stresses, σ_θ and σ_ϕ, are equal; they are given by:

$$\sigma_\theta = \sigma_\phi = -\frac{P_t}{2}\left(\frac{R_1}{r}\right)^3 + \frac{p_1}{2}\left[\left(\frac{R_1}{r}\right)^3 + 2\right] \quad (8)$$

If we use the excess magma pressure p_e (Eq. (1)) rather than the total pressure P_t, Eqs. (7) and (8) may be rewritten as:

$$\sigma_r = p_e\left(\frac{R_1}{r}\right)^3 \quad (9)$$

$$\sigma_\theta = \sigma_\phi = -\frac{p_e}{2}\left(\frac{R_1}{r}\right)^3 \quad (10)$$

For a very small chamber, with $R_1 \ll d$ and $R_1 \to 0$, but a finite $p_e R_1^3$, the intensity of the point excess pressure S of the chamber is given by $S = p_e R_1^3$, the units being Nm or work (energy). A point pressure of this kind is the basis of the "Mogi model" (Mogi, 1958), which was discussed above. From Eqs. (9) and (10) it follows that the intensity of the stress field associated with a spherical magma chamber subject to magmatic excess pressure p_e as the only loading falls of inversely as the cube of the distance (radial vector) r from the chamber. When we substitute $r = R_1$ in Eqs. (9) and (10), the compressive stress at the surface of the magma chamber becomes $\sigma_r = p_e$ whereas the tensile stress is $\sigma_\theta = \sigma_\phi = -0.5 p_e$ (Fig. 13).

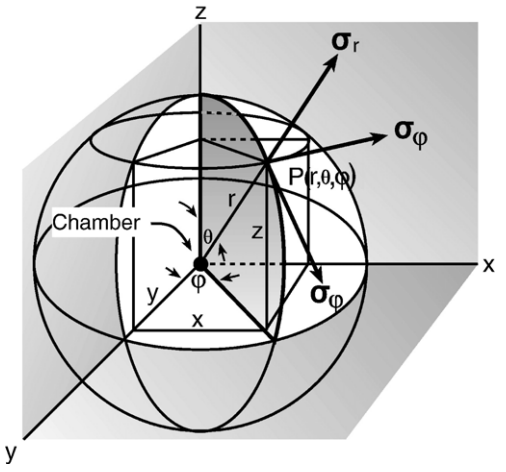

Fig. 12. Spherical magma chamber located at the origin of a spherical co-ordinate system. For a given point $P(r,\theta,\phi)$ in the crust hosting the chamber r is the radius vector, θ is the angle between the radius vector and a fixed axis, and ϕ is the angle measured around this axis. The local stress field at point P is given by the principal stresses σ_r σ_θ and σ_ϕ, where σ_r is the radial compressive stress and the tangential tensile stresses σ_θ and σ_ϕ are equal (cf. Fig. 14).

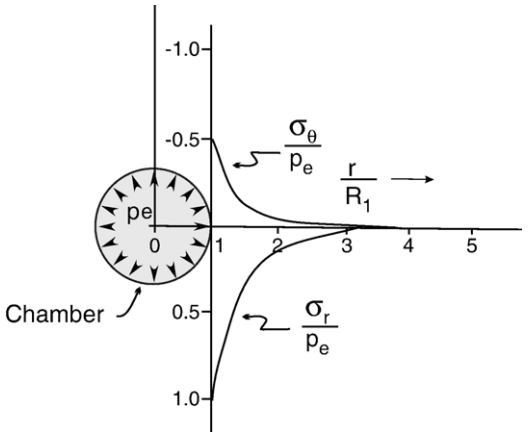

Fig. 13. Fall-off in intensity of the stresses σ_r and σ_θ away from the spherical magma chamber in Fig. 12. The stresses are measured in the vertical xz-plane and made dimensionless through dividing by the magmatic excess pressure p_e (Eq. (1)). The distance r from the chamber is also made dimensionless through dividing by the radius of the chamber R_1. At the margin of the chamber $r = R_1$ so that, from Eq. (9), the radial compressive stress σ_r is equal to the excess magma pressure whereas the circumferential tensile stress σ_θ is, from Eq. (10), half the magnitude of p_e. The stresses generated by the excess pressure p_e decrease as the cube of the distance r from the chamber and affect the strike and dip of sheet intrusions only in the vicinity of the chamber.

3.3. Cavities subject to external tension

When a spherical magma chamber is subject to external tensile stress, as is common in rift zones, the resulting stresses are very different from those generated by internal magmatic pressure. Consider a spherical magma chamber located at a considerable depth in a rift zone subject to external tensile stress $-\sigma$. In the coordinate system defined in Fig. 14, the unixial tensile loading $-\sigma$ is parallel with the z-axis (Soutas-Little, 1973). For a rift-zone magma chamber, the tensile loading direction normally coincides with that of the spreading vector, and is thus horizontal. For application to rift-zone chambers we therefore imagine that the sphere is rotated by 90° so that the z-axis becomes horizontal and parallel with the spreading vector.

The chamber is initially in a lithostatic equilibrium so that the vertical stress related to overburden pressure is balanced by the magma pressure and may, therefore, be ignored in the analysis. It follows that the only loading that needs to be considered is the tensile stress $-\sigma$. Using the coordinates defined in Fig. 14, the stresses at the surface of the sphere become (Goodier, 1933; Timoshenko and Goodier, 1970; Soutas-Little, 1973):

$$\sigma_\theta = -\frac{\sigma(27-15\nu)}{2(7-5\nu)} + \frac{15\sigma}{(7-5\nu)}\cos^2\theta \quad (11)$$

$$\sigma_\phi = -\frac{\sigma(15\nu-3)}{2(7-5\nu)} + \frac{15\nu\sigma}{(7-5\nu)}\cos^2\theta \quad (12)$$

The second terms in Eqs. (11) and (12) become zero and the tensile stresses thus maximum when $\theta=90°$. Thus, for $\theta=90°$, at the equatorial plane of the sphere, the maximum tensile stresses are:

$$\sigma_\theta = -\frac{\sigma(27-15\nu)}{2(7-5\nu)} \quad (13)$$

$$\sigma_\phi = -\frac{\sigma(15\nu-3)}{2(7-5\nu)} \quad (14)$$

At the top and bottom of the sphere, however, the external tensile stress $-\sigma$ generates compressive stress of a magnitude:

$$\sigma_\theta = \sigma_\phi = \frac{\sigma(15\nu+3)}{2(7-5\nu)} \quad (15)$$

When applied to a spherical chamber, it follows from the considerations above that the top and bottom of the sphere are along the horizontal, equatorial plane of the real magma chamber; and, similarly, that the top and bottom of the chamber lie along the equatorial plane of the sphere. Consequently, the compressive stress obtained from Eq. (15) is generated at the equatorial plane of the rift-zone chamber whereas the tensile stresses obtained from Eqs. (13) and (14) are generated at the top and bottom of the rift-zone chamber.

Simple, closed-form analytical solutions do not exist for calculating the stress concentration around a magma chamber of a general ellipsoidal form (Fig. 15). From

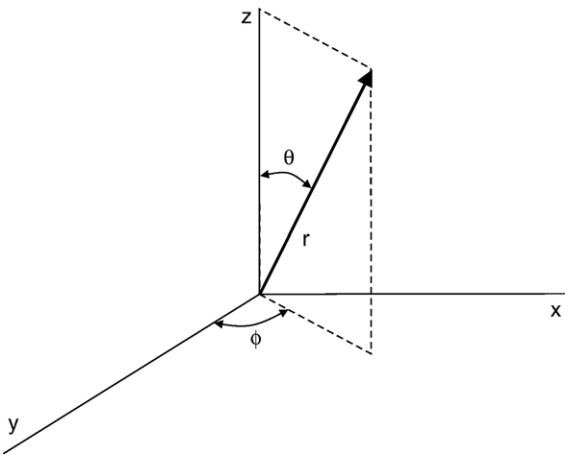

Fig. 14. The spherical coordinate system (r, θ, φ) used in Eqs. (11)–(15) (cf. Fig. 12).

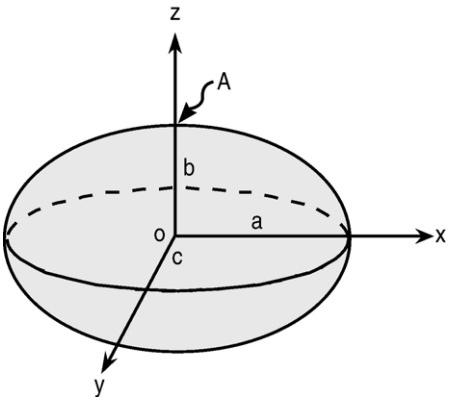

Fig. 15. General ellipsoidal magma chamber where all the semi-axes may be of different lengths ($a \geq b \geq c$). The stress concentration at point A is given in Fig. 17.

equations derived by Sadowsky and Sternberg (1947, 1949) for three-dimensional ellipsoidal cavities, however, some estimates of the stress concentrations around deep-seated ellipsoidal magma chambers can be made (Gudmundsson, 1988). If a two-axial, prolate ellipsoidal magma chamber has horizontal width $2c$, height (vertical or dip dimension) $2b$, and length (strike dimension) $2a$, the ratio c/b is referred to as the shape ratio of the magma chamber. For a two-axial chamber, the dimension a is equal to either c or b. The focus is on the uppermost part of the chamber where, as before, rupture and dyke injection is most likely to take place.

Here the tensile stress concentration at the top of the prolate ellipsoidal magma chamber is calculated for host rocks with different Poisson's ratios: 0.25 and 0.30 (Fig. 16). For the special case when $c/b=1$ and $a=1$, the chamber is spherical and the tensile stress concentration can be calculated from Eqs. (13) and (14).

When the chamber has the shape of a triaxial ellipsoid, so that $a \geq b \geq c$ (Fig. 15), the stress concentration factor k at point A on the ellipsoidal magma chamber can be calculated (Fig. 17). For a triaxial magma chamber that is elongate parallel with a divergent plate boundary or a rift zone, two-dimensional (hole) models may often be used to calculate the stress concentration. For example, if the length of the chamber parallel with the axis of the rift zone, that is, the strike dimension of the chamber, is much greater than its height, that is, its dip dimension (so that $2a \gg 2b$), the tensile stress at point A at the top of the chamber can be calculated approximately using the two-dimensional formula:

$$\sigma_3 = -\sigma\left[\frac{2b}{c} + 1\right] \quad (16)$$

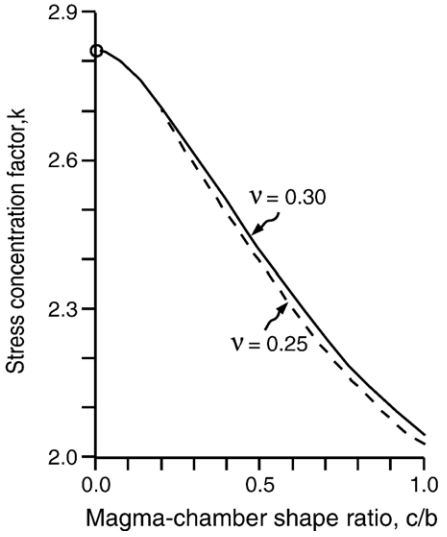

Fig. 16. Many magma chambers are stock-like, in which case a cylinder or a prolate ellipsoid with a vertical long axis may be an appropriate model. Here the tensile stress concentration factor k for the top of a prolate ellipsoidal chamber is presented. The factor k is given as a function of the shape ratio c/b ($c/b=1.0$ for a spherical chamber) and for two values of Poisson's ratio ν. The ratio $\nu=0.25$ is appropriate for the host rocks of most shallow crustal chambers; $\nu=0.30$ may be suitable for chambers (reservoirs) in the lower crust or upper mantle.

Here, σ_3 is the maximum principal tensile stress, which occurs at point A, and $-\sigma$ is the remote tensile stress related to plate pull. For example, for $c/b=0.1$ and a very elongate chamber ($b/a\approx 0.0$), Eq. (16) gives $\sigma_3=-21\sigma$, in agreement with Fig. 17). Eq. (16) is similar to the one used to calculate tensile stresses at elliptical holes subject to fluid overpressure P_0 (then P_0 is substituted for $-\sigma$ and the term +1 in Eq. (1) becomes − 1), and is widely applied in studies of fractures (Maugis, 2000; Sanford, 2003).

4. Stresses nearby chambers — analytical models

Stress concentrations associated with a magma chamber are normally confined to the host rocks at and nearby the margin of the chamber. At distances similar to or greater than the diameter of the chamber, the stresses become similar to that of the host rock without the chamber (Fig. 13). These results follow from Eqs. (7) to (10) which show how the stress intensity falls off with distance from a spherical magma chamber.

Some composite volcanoes may have chambers with the shape of a vertical cylinder. In particular, chambers of this shape are likely to be partly responsible for the commonly inferred (primarily) lateral dyke propagation in some volcanic edifices and regional dyke swarms (Rubin, 1995; Fialko and Rubin, 1999; Ernst et al., 2001; Mege and Korme, 2004; Pinel and Jaupart, 2004; Klugel et al., 2005; Acocella et al., 2006a, b). Extinct chambers, plutons, of this shape are referred to as plugs or necks when the diameter is from metres to a few thousand metres and as stocks for larger diameters; the largest diameters are 10–11 km. In Iceland, several plugs are known from eroded composite volcanoes (e.g., Walker, 1963).

The stress field around a plug-like magma chamber follows, approximately, from the model of a cylinder (Fig. 18) of an inner radius R_1 and outer radius R_2. Since the radius of the composite volcano with the plug-like chamber is very much larger than the radius of the plug, we have $R_2 \gg R_1$ and may assume that R_2 is effectively infinite. We use polar coordinates where the radius vector is denoted by r and the polar angle by θ. At its margin, R_1, the chamber is under total magma pressure P_t (Eq. (1)) whereas the composite volcano is subject to horizontal compressive stress σ_H at R_2. For isotropic state of stress, the maximum (σ_H) and the minimum (σ_h) horizontal compressive stresses are equal. Then the

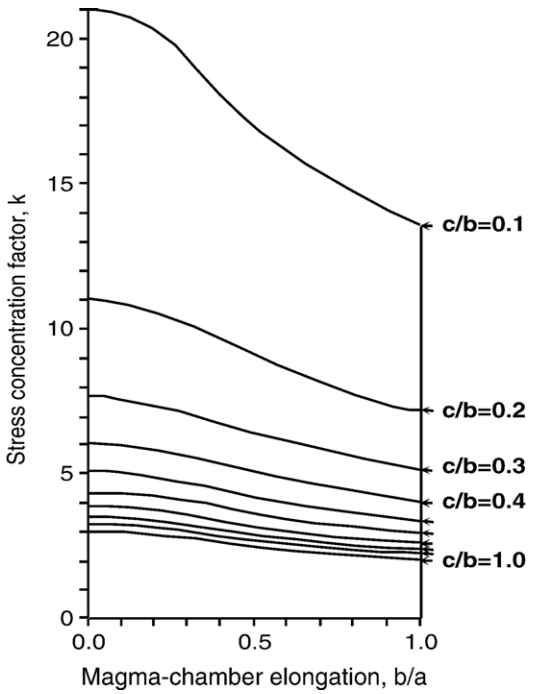

Fig. 17. Tensile stress concentration, represented by the factor k, at point A on the general ellipsoidal chamber in Fig. 15. The stress concentration is given for various ratios of the axes c/b (shape ratio, cf. Fig. 16) and b/a (elongation). For example, when $c/b=1.0$ the chamber has a circular, vertical cross-sectional area; then if the chamber is also very long in relation to its other dimensions, so that $a\gg b$ and $b/a\rightarrow 0.0$ the stress concentration factor at A is 3.0 (cf. Eq. (16)). If $c/b=b/a=1.0$, so that $a=b=c$, the chamber is spherical and, for point A, $k=2.02$ (for $\nu=0.25$; cf. Fig. 16).

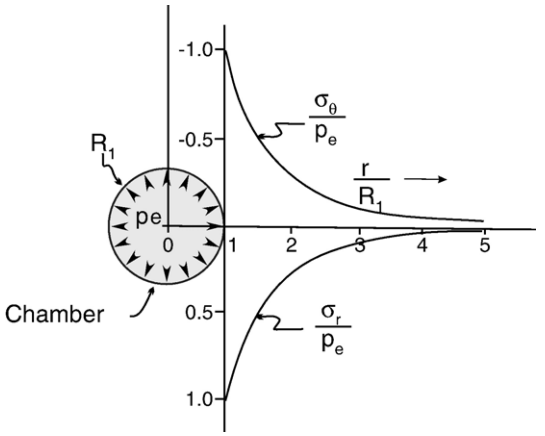

Fig. 18. Decrease in radial σ_r and circumferential σ_θ stress with distance from a plug-like (cylindrical) magma chamber. The stresses are made dimensionless through dividing by the magmatic excess pressure p_e, defined in Eq. (1). The distance r from the chamber is also made dimensionless through dividing the radius vector r, measuring the distance from the chamber centre, by the chamber radius R_1 (the outer radius R_2 of the crustal segment hosting the chamber is effectively infinite and is not shown). At the margin of the chamber $-\sigma_\theta=\sigma_r=p_e$.

radial compressive stress σ_r is (Saada, 1983; Gudmundsson, 2002):

$$\sigma_r = P_t\left(\frac{R_1}{r}\right)^2 + \sigma_H\left[1-\left(\frac{R_1}{r}\right)^2\right] \quad (17)$$

Similarly, the tangential or circumferential tensile stress σ_θ is:

$$\sigma_\theta = -P_t\left(\frac{R_1}{r}\right)^2 + \sigma_H\left[1+\left(\frac{R_1}{r}\right)^2\right] \quad (18)$$

Eqs. (17) and (18) can be simplified when the excess magmatic pressure p_e is used rather than the total magmatic pressure P_t (Fig. 18). In this case, the excess pressure is the difference between the total magmatic pressure in the cylindrical chamber and the regional horizontal compressive stress σ_H. Eq. (1) indicates that the chamber will rupture and inject dykes when $p_e=T_0$, where T_0 is the tensile strength of the host rock at the chamber margin. If σ_H is equal to the lithostatic stress in the crust hosting the chamber, then $\sigma_H=\sigma_h=p_1$. Substituting p_e for P_t and putting $\sigma_H=0$ in Eqs. (17) and (18), the radial compressive stress becomes:

$$\sigma_r = p_e\left(\frac{R_1}{r}\right)^2 \quad (19)$$

Similarly, the circumferential tensile stress becomes:

$$\sigma_\theta = -p_e\left(\frac{R_1}{r}\right)^2 \quad (20)$$

Clearly, Eqs. (19) and (20) indicate that the intensity of the stress field generated by an excess pressure p_e in a vertical, cylindrical magma chamber falls off as the square of the distance r from the margin of the chamber (Fig. 18). These results are similar to those for a spherical magma chamber (Fig. 13). They show that during unrest periods with inflation of a magma chamber, the condition of dyke injection and propagation are commonly met at, and in the vicinity of, the magma chamber while the condition of dyke arrest are met at a certain distance from the chamber.

5. Stresses nearby chambers — numerical models

5.1. Homogeneous, isotropic host rock

The analytical models presented above assume the crust holding the chamber to be homogeneous and

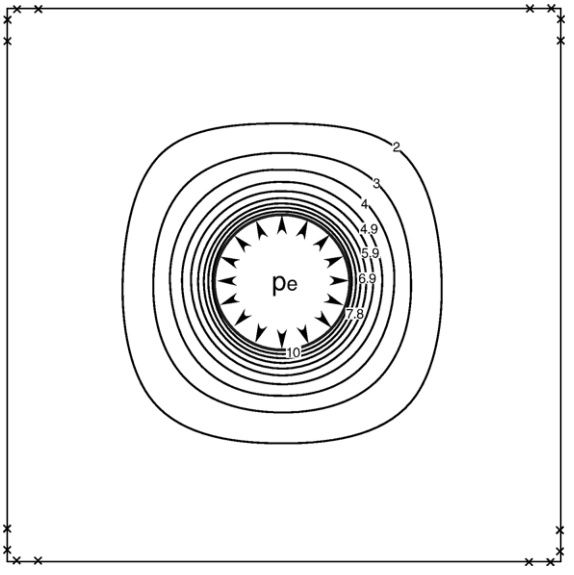

Fig. 19. Contours of the maximum principal tensile stress σ_3, in megapascals, around a magma chamber of circular cross section subject to excess pressure $p_e=10$ MPa as the only loading (modified from Gudmundsson and Brenner, 2005). The homogeneous and istotropic host rock has a stiffness of 10 GPa. The crosses indicate the boundary conditions of no displacement in the model. In the model the diameter of the chamber is 0.25 units, whereas the height of the model is one unit; the chamber diameter would thus be 2.5 km, and the depth to its top 3.75 km, in a rift zone of thickness 10 km. The tensile stresses diminish rapidly with distance from the chamber margin (cf. Eqs. (9), (10), (19), (20) — the latter two apply directly to this two-dimensional model). The σ_3-contours approach a square shape with increasing distance from the chamber because of the square shape of the modelled elastic plate.

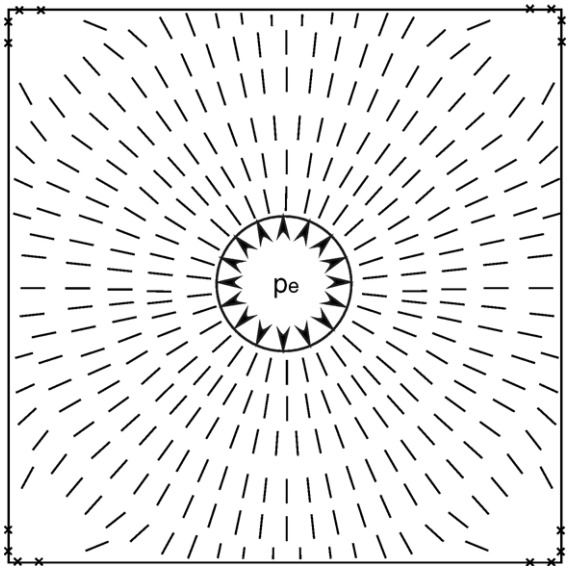

Fig. 20. Stress field around a magma chamber of circular vertical cross-section subject to internal magmatic excess pressure $p_e = 10$ MPa (modified from Gudmundsson and Brenner, 2005). In this finite-element model, the ticks represent the trajectories of the maximum principal compressive stress σ_1 along which ideal dykes and inclined sheets, injected from the chamber, would propagate. The model corresponds approximately to that in Fig. 19.

isotropic. Numerical models of magma chambers based on such assumptions indicate the general stress concentrations and the stress trajectories around the chambers. All the numerical models in this paper were made using the finite-element program ANSYS and the boundary-element program BEASY. A description of the boundary-element method in general, and that of the BEASY program in particular, is given by Brebbia and Dominquez (1992) and the BEASY homepage (www.beasy.com). Similarly, a general description of he finite-element method is provided by Zienkiewicz (1977) and that of the ANSYS program by Logan (2002) and the ANSYS homepage (www.ansys.com). Jing and Hudson (2002) discuss the various numerical methods, including the boundary element and the finite element, in context of solving rock-mechanics problems. The rock stiffnesses used in the models are obtained either directly from laboratory tests (Carmichael, 1989; Afrouz, 1992; Bell, 2000; Myrvang, 2001), or modified using information on in-situ properties (Farmer, 1983; Priest, 1993; Schön, 2004). The boundary conditions used in the models, as specified below, are obtained from the appropriate geological and geophysical field studies.

The most basic of these models is the one of a magma chamber in a crustal segment that is very large in comparison with the size of the chamber itself. A two-dimensional version of this model shows the stress concentration (Fig. 19) and the potential paths of dykes injected from the magma chamber, that is, the trajectories of the maximum compressive principal stress σ_1 (Fig. 20). In this and all subsequent numerical models in this paper, the models are fastened at some or all the corners, using the conditions of no displacement, so as to avoid rigid-body rotation and translation. Numerical models with smaller chambers, that is, models with larger computational domains, yield stress results that are similar to those obtained in the models in the present paper.

The stress field around magma chambers in a homogeneous, isotropic crust depends on the chamber location and shape, and its tectonic environment. For example, when the chamber is near the surface of its volcano, the sites of maximum tensile stress concentration at the margin of the chamber shift towards the upper part of the chamber (Fig. 21). The reason for the shift in location of stresses is the vicinity of the earth's free surface. For a chamber close to the surface, the resistance to elastic deformation of the chamber margin is less in the direction of the surface than in any other direction. Consequently, the deformation and stress shift towards the upper margin of the chamber. The trends of the resulting dykes, however, are not much affected (Gudmundsson, 2002).

The loading conditions can have strong effects not only on the location of the sites of maximum stress concentrations around the chamber, but also on the trends of the injected dykes. When, for instance, a shallow magma chamber is primarily loaded by external tension, as is common at divergent plate boundaries and in rift zones, the main tensile stress concentration occurs

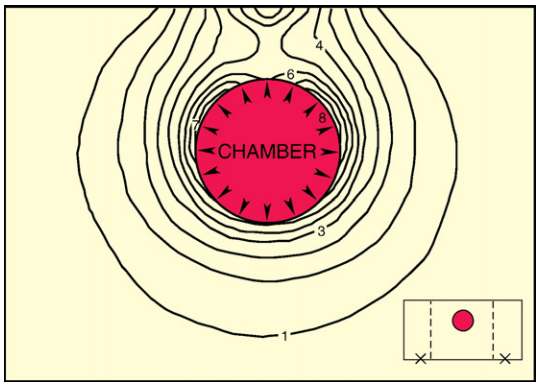

Fig. 21. Stress field, indicated by the contours of maximum principal tensile stress σ_3 in mega-pascals, around a shallow magma chamber. In this boundary-element model, the chamber is of a circular cross-section and subject to internal magmatic excess pressure $p_e = 5$ MPa. Modified from Gudmundsson (1998).

at the top of the chamber (Fig. 22). Also, the potential paths of the dykes injected from the chamber are mostly vertical (Fig. 23). By contrast, the potential paths of sheets injected from a chamber subject to magmatic excess pressure as the primarily loading are mostly inclined (Fig. 20). It should be emphasised, however, that the loading conditions, rather than the tectonic processes giving rise to them, are of main importance for magma-chamber rupture and dyke injection. For example, for a magma chamber subject to extension, the tensile stress concentration around the chamber, and the eventual rupture of the chamber, does not depend much on whether the extensional regime is associated with transtension along a major strike-slip fault or with rifting at a divergent plate boundary.

The shape of a magma chamber also affects the location of the main stress concentration around it, as well as the potential paths of the injected dykes and sheets (Fig. 24). Thus, for a sill-like (oblate ellipsoidal) and comparatively shallow chamber subject to excess magmatic pressure as the only loading, sheet injection tends to occur at the sites of maximum tensile stress concentration, namely at the upper lateral ends of the chamber (Fig. 24), and there the sheet dip is shallow.

A homogeneous, isotropic crust, however, does not really exist. Models where the crust is assumed homogeneous and isotropic give certain ideas as to stress fields around magma chambers and associated emplacement of dykes. But such models are not suitable for the detailed analysis of dyke paths. Furthermore, in a homogeneous, isotropic crust most buoyant magma-driven fractures should reach the surface to supply magma to eruptions. By contrast, field observations show that most dykes become arrested; they never reach the surface

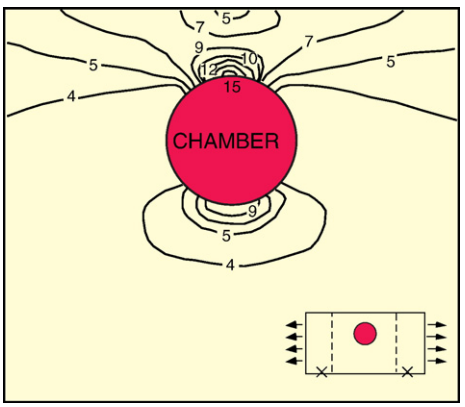

Fig. 22. Contours of the maximum principal tensile stress σ_3, in megapascals, around a magma chamber of circular vertical cross-section subject to external, remote horizontal tensile stress (plate pull) of 5 MPa as the only loading (modified from Gudmundsson, 1998).

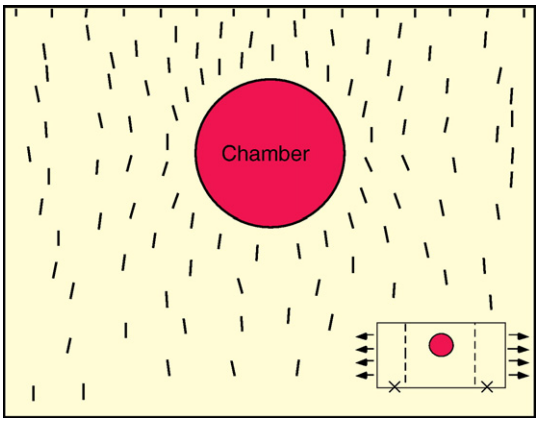

Fig. 23. Trajectories of the maximum principal compressive stress σ_1 around the chamber model in Fig. 22 (modified from Gudmundsson, 1998). Ideal dykes and inclined sheets, injected from the chamber, would propagate along these trajectories and be mostly subvertical (cf. Fig. 20).

to feed eruptions (Harris et al., 2000; Gudmundsson, 2002, 2003; Stewart et al., 2003, 2005; Gudmundsson and Brenner, 2005; Gudmundsson and Philipp, in press).

5.2. Heterogeneous, anisotropic host rock

To understand how the local stress fields around magma chambers may encourage dyke arrest, we must use numerical methods. This follows primarily because not only are the stress fields complex, but the mechanical properties of the rock layers that host the magma chambers are normally highly variable (Carmichael, 1989; Bell, 2000; Myrvang, 2001; Gudmundsson, 2002, 2003; Schön, 2004). When subject to loading, soft pyroclastic rocks, for example, behave very differently from stiff basaltic lava flows or sills, and both types are common host rocks of magma chambers in composite volcanoes. There are thus abrupt changes in mechanical properties of the layers that constitute composite volcanoes, and through which dykes must propagate on their paths to the surface. These abrupt changes in properties are the main reasons for the complex stress fields of composite volcanoes and for dyke arrest. To explore the effects of these stress fields on dyke emplacement, we consider several numerical models of local stresses around single and double magma chambers of different shapes and located in composite volcanoes or crustal segments whose layers have contrasting stiffnesses.

The stiffnesses used in the numerical models are based on the following considerations. Laboratory measurements indicate that layers of basalt, such as lava flows, and gabbro, such as large intrusions – for example,

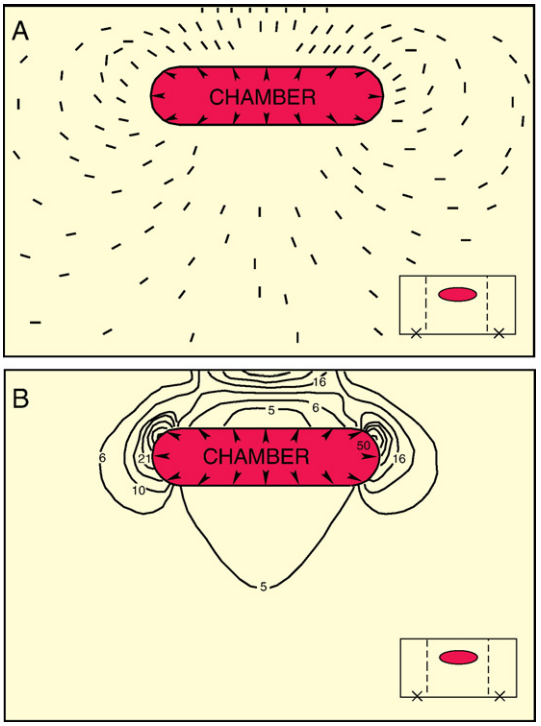

Fig. 24. Stress field around a shallow, sill-like magma chamber subject to internal magmatic excess pressure p_e=5 MPa as the only loading (modified from Gudmundsson, 1998). A) The ticks represent the trajectories of the maximum principal compressive stress σ_1 along which ideal dykes and inclined sheets, injected from the chamber, would propagate. B) The contours indicate the maximum principal tensile stress σ_3 in mega-pascals.

solidified parts of mafic magma chambers (Fig. 25) – reach stiffnesses of 110–130 GPa; volcanic tuffs, by contrast, have stiffnesses as low as 0.05–0.1 GPa (Afrouz, 1992; Bell, 2000). More extreme values are known, however. For example, some rocks reach stiffnesses of up to 150–200 GPa (Myrvang, 2001). By contrast, unconsolidated rocks may have static stiffnesses as low as 0.08 GPa for sand and gravel and 0.003 GPa for clay (Schön, 2004). Poisson's ratios of the rocks that commonly constitute composite volcanoes, however, have a much narrower range. Poisson's ratio of many basaltic lava flows is, for instance, the same as that of many volcanic tuffs, or about 0.25 (Bell, 2000).

In Iceland, most active composite (central) volcanoes contain high proportion of hyaloclastite (moberg), a pyroclastic rock made of basaltic breccias and tuffs formed in subglacial and submarine eruptions. Static laboratory stiffnesses of young hyaloclastites are mostly between 0.5 GPa and 8 GPa (Jonsson, 1971; Oddson, 1984; Egilsson et al., 1989). Sedimentary rocks, mainly tillites of late Pleistocene age which are common outside and inside the composite volcanoes, have similar stiffnesses whereas, as indicated above, unconsolidated sediments, common in some composite volcanoes and rift zones, have much lower stiffnesses (Schön, 2004). Near-surface Holocene and Pleistocene basaltic lava flows have static stiffnesses mostly between 10 GPa and 35 GPa

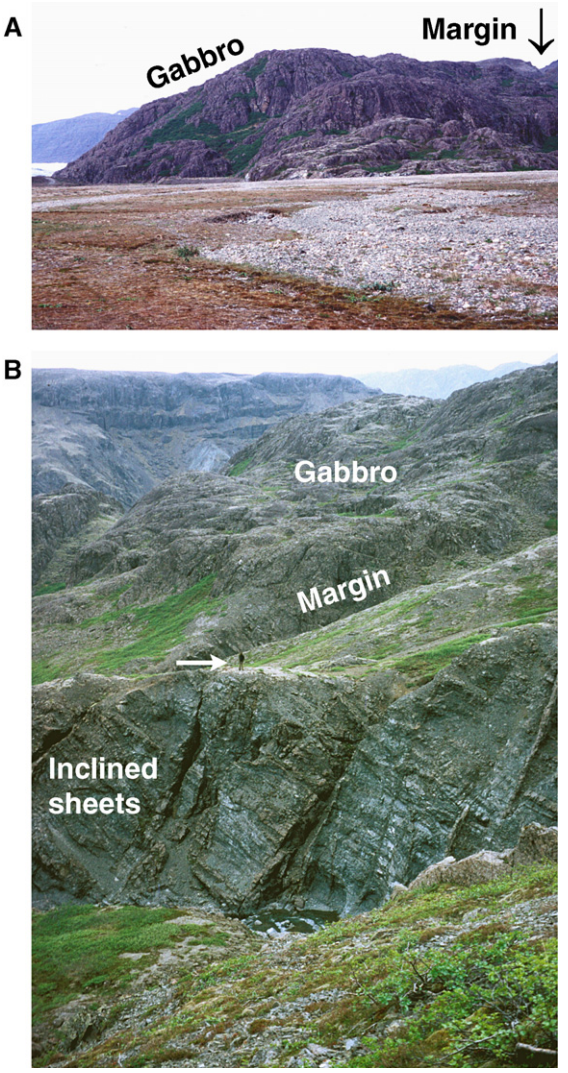

Fig. 25. Parts of the shallow magma chamber (of grabbro) and the swarm of dykes and inclined sheets in the Geitafell Volcano, an extinct Tertiary composite volcano in Southeast Iceland (Torfason, 1979; Fridleifsson, 1983). A) View north, the gabbro pluton forms the uppermost part of the extinct magma chamber, currently exposed at a depth of nearly 2 km beneath the initial top of the original volcano. The indicated margin (also in B) marks the boundary between the gabbroic magma chamber and the inclined sheet swarm. B) View west, in the high-intensity part of the sheet swarm next to the contact with the gabbro 80–100% of the rock consists of inclined sheets, mostly about 0.5 m thick, that form a single mechanical unit. A person, indicated by a white arrow, provides a scale.

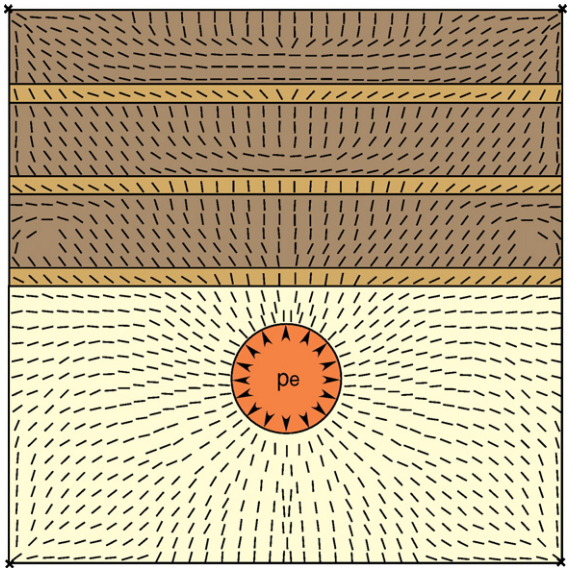

Fig. 26. Stress field around a magma chamber of circular vertical cross-section located in a layered crustal segment of a composite volcano. The chamber itself is hosted by a layer with a stiffness of 40 GPa. By contrast, the thin layers above the chamber are very soft, with a stiffness of 1 GPa, whereas the thick layers are very stiff, with a stiffness of 100 GPa. In this finite element model, the chamber is subject to internal magmatic excess pressure of $p_e = 5$ MPa. The ticks represent the trajectories of the maximum principal compressive stress σ_1 along which ideal dykes and inclined sheets, injected from the chamber, would propagate.

(Oddson, 1984; Egilsson et al., 1989). The stiffnesses of these rocks generally increase with age and depth of burial.

The first two layered models (Figs. 26 and 27) show the effects of magma-chamber geometry on the local stresses in a composite volcano. The magma chamber itself is located in a rock unit of a stiffness typical for the crust at the depth of a few kilometres, 40 GPa, whereas the layers above that unit form a part of the composite volcano and alternate between being very soft, 1 GPa, and very stiff, 100 GPa. This is a very large variation in stiffness, but still well within the limits obtained in laboratory measurements, as indicated above. The very soft layers may represent tuffs, sediments, scoria and soils between lava flows whereas the very stiff layers represent basaltic and intermediate lava flows and intrusions.

In the first layered model, a magma chamber of a circular cross section is subject to internal excess magmatic pressure of 5 MPa as the only loading (Fig. 26). This excess pressure is chosen so as to be similar to the in situ tensile strength of a typical crystalline host rock, normally 0.5–6 MPa (Schultz, 1995; Amadei and Stephansson, 1997). The size of the chamber in relation to the crustal segment and layer thickness is as indicated in Fig. 26. The chamber is located in a crustal segment consisting of seven layers of very different stiffnesses; 1 GPa (the thin layers), 40 GPa (the layer hosting the chamber), and 100 GPa (the thick layers). The same layer stiffnesses and magmatic pressure are used in the model in Fig. 27, the only difference being the geometry of the chamber.

Comparison of the two models (Figs. 26 and 27) shows the effect of magma-chamber geometry on the local stress field, as represented by the trajectories of the maximum principal compressive stress σ_1. Since ideal dykes tend to follow the σ_1-trajectories, those injected from the circular chamber in Fig. 26 would be steeply inclined or vertical up to the upper contact between the central thin soft layer and the second thick layer. There the σ_1-trajectories abruptly become horizontal, in which case the propagating dykes might change into sills. This follows since most dykes are extension fractures so that if a dyke is to continue its propagation in a part of a crustal segment where σ_1 is horizontal, it would have to propagate in that part as a horizontal sill. More likely, however, on meeting a part of a layer or a contact where σ_1 is horizontal, a dyke would become arrested. In the marginal upper parts of the model, however, the σ_1-trajectories remain inclined through all the layers, making it possible for some inclined sheets to reach the uppermost layer and, perhaps, the surface.

For the sill-like chamber (Fig. 27) the abrupt change from vertical to horizontal σ_1-trajectories occurs already

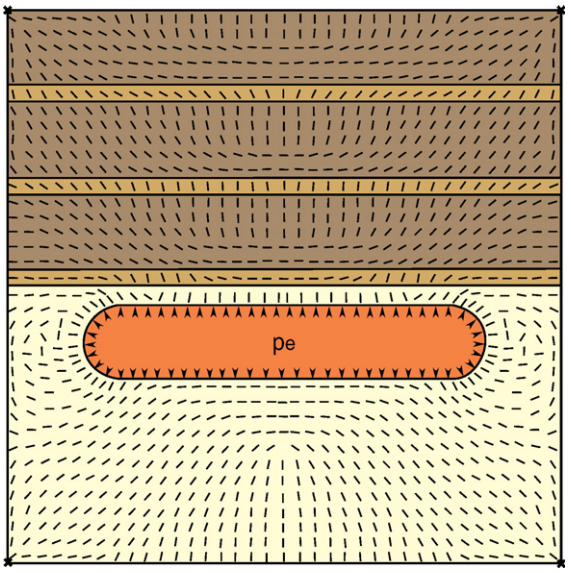

Fig. 27. Stress field around a sill-like magma chamber located in a layered crustal segment of a composite volcano. In this finite-element model, the layers have the same properties, and the loading conditions are the same, as in the model in Fig. 26. The ticks represent the trajectories of the maximum principal compressive stress σ_1.

in the first soft layer above the magma chamber. Thus, for the given layering and loading conditions, the difference in geometry between the chambers in Figs. 26 and 27 results in very different local stress fields. And these different local stress fields, in turn, encourage different dyke-injection paths during unrest periods. In particular, for the sill-like geometry (Fig. 27) most dykes injected from the upper central part of the chamber would become arrested just above its margin, whereas some inclined sheets injected from near its lateral ends might propagate to shallower depths in the crust, possibly reaching the surface to feed eruptions.

Many shallow magma chambers in Iceland and elsewhere are at depths of only 1.5–2 km below the surface of the associated volcano. For a chamber with a top at 1.5 km depth, the stiff layers in the models in Figs. 26 and 27 would be about 380 m thick each and the thin, soft layers about 90 m. In Iceland, hyaloclastite layers forming parts of mountains and the thickest basaltic (pahoehoe) lava flows may reach thicknesses of several hundred metres. The thicknesses of most layers constituting composite volcanoes and rift zones, however, are of the order of tens of metres or less rather than hundreds of metres.

To study the effects of thinner layers, a 30-layer model was made (Fig. 28). For a shallow circular chamber with a top at 1.5 km depth, the thickness of each of the 30 layers would be 50 m, similar to that of many pyroclastic and sedimentary layers and thick lava flows. As in the models above, the alternate layers have stiffnesses of 1 GPa and 100 GPa whereas the chamber excess pressure here is 10 MPa. The results (Fig. 28) show that abrupt stress changes occur at many contacts between soft and stiff layers, particularly in the central part of the model above the chamber. Thus, for these loading conditions and rock-mechanical properties many dykes injected during unrest periods would tend to become arrested and eruptions prevented. The results also support the general conclusion based on field studies of dykes in eroded composite volcanoes (Gudmundsson, 2002, 2003; Gudmundsson and Brenner, 2005; Gudmundsson and Philipp, 2006) and theoretical studies of composite materials (Daniel and Ishai, 1994; Tan, 1994; Kaw, 1997; Hyer, 1998) that contrasts in mechanical properties between layers rather than absolute layer thicknesses control the local stresses at layer contacts and, thereby, dyke arrest.

Although near-surface layers may be horizontal in composite volcanoes, and particularly in rift zones, more commonly the layers are inclined (Figs. 4 and 5). In composite volcanoes that form topographic highs, the uppermost layers may be outward dipping, but become inward dipping at certain depths (Fig. 5). The same applies to rift zones. The inward dip is primarily due to the additional load generated by the extrusive and intrusive rock which leads to gradual down-bending of the associated crustal segment. For example, in the palaeorift zones in Iceland the dips of the lava flows increase, on average, about 1° for every 150 m of crustal

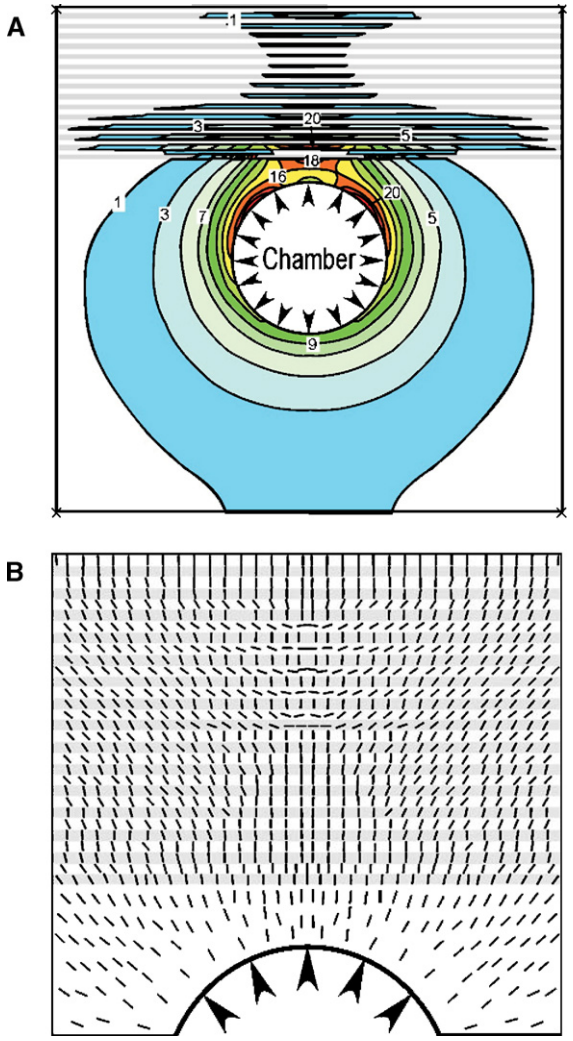

Fig. 28. Stress field around a magma chamber of a circular vertical cross section located in a crustal segment with 30 layers. In this finite-element model the only loading is magmatic overpressure of 10 MPa in the chamber. The 30 layers above the layer hosting the chamber itself have stiffnesses of 1 GPa and 100 GPa. A) The magnitudes, in mega-pascals, of the maximum tensile principal stress σ_3 (for values exceeding 1 MPa) indicate that the tensile stresses concentrate in the stiff layers. B) The trajectories of the maximum principal compressive stress σ_1 in the rocks above the uppermost part of the chamber in A. The illustration indicates in detail how the direction of σ_1 changes from vertical (favouring dyke propagation) to horizontal (favouring dyke arrest) at layer contacts.

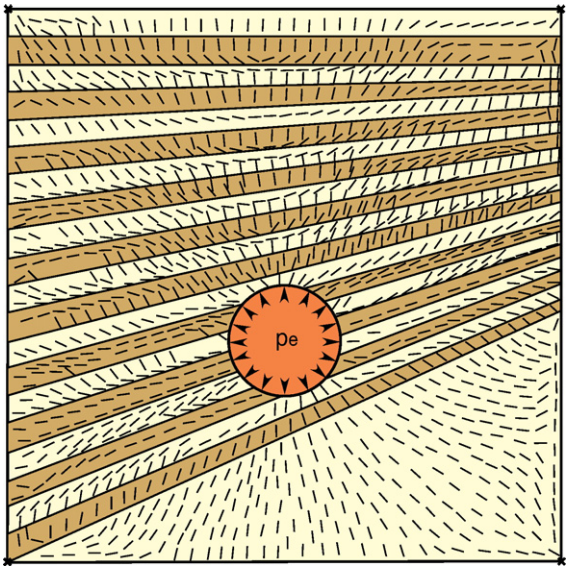

Fig. 29. Stress field around a magma chamber located in a layered crustal segment where the layers have different stiffnesses and are also dipping (cf. Fig. 4). In this finite-element model, the chamber is of a circular, vertical cross section and has a magmatic overpressure of 5 MPa as the only loading. The layered segment is composed of 20 comparatively thin layers, the magma chamber itself being located in 7 layers, and one thick layer below the main layered part. For a chamber with a top at 1.5 km depth, each layer would be about 100 m thick. The yellow layers are soft, with a stiffness of 1 GPa, the brown layers are stiff, with a stiffness of 100 GPa, and the thick yellow bottom layer has a stiffness of 40 GPa. The dip of the layers increases with depth in the crust, as is commonly observed (Fig. 4)). The ticks show the trajectories of the maximum principal compressive stress σ_1 which rotates from vertical (favouring dyke propagation) to horizontal (favouring dyke arrest) at many layer contacts in the central part above the magma chamber.

depth (Fig. 4). At depth the layers thus dip towards the centre of the composite volcano or the axis of the rift zone. In many deeply eroded composite volcanoes the centres towards which the layers dip are occupied by plutons that represent the uppermost parts of the extinct, shallow chambers of the volcanoes ((Figs. 8, 9, 25)).

The effects of the gradual tilting of the layers with depth in composite volcanoes and rift zones is considered in the model in Fig. 29. The stiffnesses are the same as in the previous models, 1 GPa for the soft layers and 100 GPa for the stiff layers. The magma chamber is 2.5 units in diameter, or 2.5 km in a 10-km-thick crust, and the only loading is a magmatic excess pressure of 5 MPa. It should be noted that the geometries of the stresses are not much dependent on whether the magmatic excess pressure is 5 MPa or 10 MPa.

In the central part of the crustal segment above the top of the magma chamber the σ_1-trajectories close to and at the contacts between the stiff and the soft layers are subparallel to the contacts. On entering these local stress fields, propagating dykes would thus tend to change into sills (Fig. 2) or stop altogether, that is, become arrested. Also, the dykes that nevertheless make it to the surface would not reach it above the top of the chamber but in an area shifted in the dip-direction of the lava pile (Fig. 30). Thus, tilting of the lava pile may be one reason for the common shifting of the volcanic systems in the down-dip direction of the lava pile — as is well known from Iceland (Helgason, 1985).

Many and perhaps most composite volcanoes are supplied with magma through double magma chambers. A shallow chamber is then fed by a deep-seated chamber, located in the lower crust or at the crust–mantle boundary (Fig. 5). Here I present two numerical models of a double magma chamber located in a layered crust (Figs. 31 and 32). The models are identical except for the loading conditions. The crustal segment hosting the shallow sill-like chamber is 6–7 km thick, and thus appropriate for fast-spreading ridges such as the East Pacific Rise. The shallow chamber is supplied with magma from a deeper, flat reservoir, located at the bottom of the crustal segment. The stiffnesses of the layers gradually increase with depth, from 10 GPa for the surface layer to 50 GPa for the bottom layer, that is, the roof of the deeper reservoir. Also, in accordance with observations, all the layers dip towards the centre of the

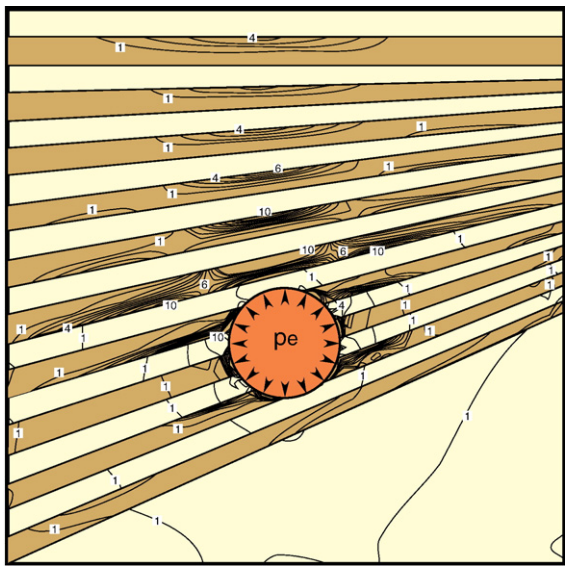

Fig. 30. Stress field around the magma chamber in Fig. 29 represented by the contours of the maximum tensile principal stress σ_3 in megapascals (cf. Fig. 4). Only those dykes that propagate within the region of maximum tensile stress (concentrated in the stiff, brown layers) have a chance of reaching the surface. Dyke-fed volcanic fissures forming a volcanic system at the surface would therefore not be right above the centre of the chamber, but rather shifted somewhat in the down-dip direction of the crustal segment, that is, to the left.

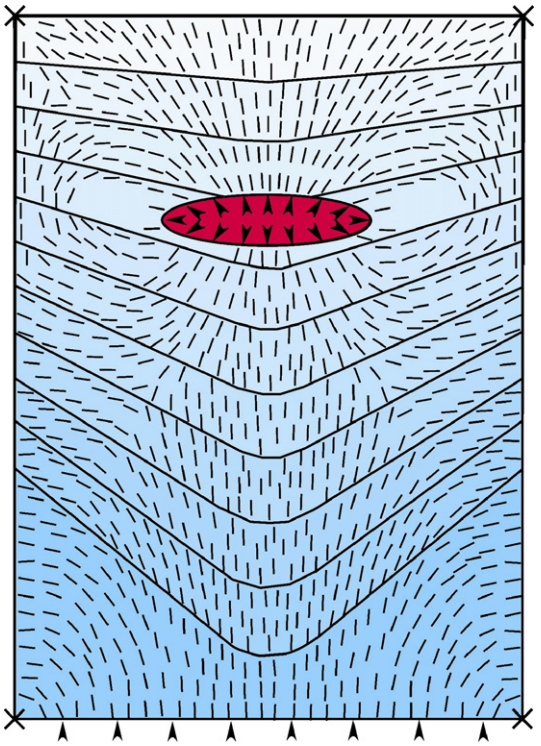

Fig. 31. Stress field around a double magma chamber in a layered crustal segment of arbitary thickness. Both chambers are sill-like; the upper one (red) is shown as a sill, the lower one (the source reservoir) as a flat roof. The shallow chamber and the lower reservoir are both subject to magmatic excess pressure of 5 MPa; this is the only loading in this finite-element model. The model consists of 11 layers that gradually increase in dip and stiffness with depth, as is commonly observed in composite rift zones and volcanoes (Fig. 4). The uppermost layer has a stiffness of 1 GPa, the bottom layer 50 GPa. The ticks represent the trajectories of the maximum principal compressive stress σ_1 along which ideal dykes and inclined sheets, injected from the chamber, would propagate. Compare Figs. 24 and 32.

composite rift zone and the dips gradually increase with depth.

The local stresses, as indicated by the σ_1-trajectories, are very different in the two models. In the model in Fig. 31 the only loading is internal magmatic excess pressure of 5 MPa, both in the deep-seated reservoirs as well as in the shallow chamber. The σ_1-trajectories tend to be somewhat inclined above the marginal part of the deep-seated reservoir, but much more so in the vicinity of the shallow chamber. By contrast, when the only loading is external tension of 5 MPa, the σ_1-trajectories remain mostly vertical and largely unaffected by the shallow chamber (Fig. 32).

These results are in agreement with those obtained in earlier models of shallow magma chambers (Figs. 20, 23, 24)). Clearly, when the primary loading is internal magmatic excess pressure, the shape of the shallow chamber has great effects on the σ_1-trajectories and, therefore, the propagation directions of the dykes. By contrast, when the principal loading is external tension, as is common during many rifting episodes at divergent plate boundaries, the σ_1-trajectories tend to be roughly perpendicular to the direction of the spreading vector, that is, the local trend of σ_3, and therefore subvertical. Thus, loading through excess magmatic pressure tends to favour inclined sheets whereas loading through external tension tends to favour subvertical dykes.

6. Dyke injection from a deep-seated reservoir

Consider first elongate magma reservoirs of the type that presumably underlie large parts of the rift-zone volcanic systems such as at divergent plate boundaries in general and in the rift zone of Iceland in particular (Figs. 5, 10, 33). The conditions for reservoir rupture and dyke injection, given by Eq. (1), are presumably commonly reached through reduction of σ_3 in the roof of the reservoir. This reduction is directly related to plate movements which generate relative or absolute tensile stress concentrations in the reservoir roof as a consequence of its shape and plate pull (Eq. (16)).

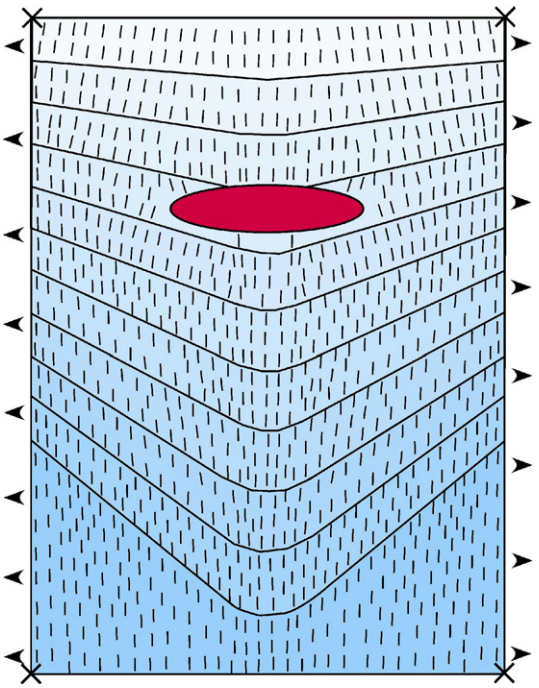

Fig. 32. Stress field around a double magma chamber in a layered crustal segment. The same model as in Fig. 32 except that the loading conditions are different. Here the entire crustal segment is subject to a horizontal tensile stress (plate pull) of 5 MPa as the only loading. The ticks represent the trajectories of the maximum principal compressive stress σ_1 along which ideal dykes and inclined sheets, injected from the chamber, would propagate. Compare Figs. 24 and 31.

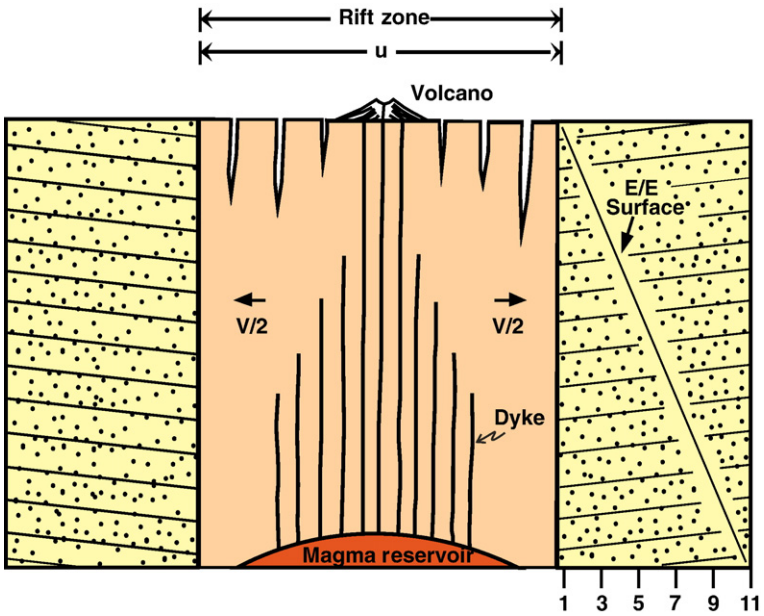

Fig. 33. Rift zone of width u is subject to a tensile strain generated by plate pull with a total spreading rate v. The rift zone is underlain by a sill-like (flat) magma reservoir (red) which injects dykes at a frequency determined by Eq. (25). The lava flows outside the rift zone (yellow parts) dip towards its axis and their stiffnesses in relation to the stiffness at the surface ($E/E_{surface}$) gradually increase with depth.

The one-dimensional Hooke's law in elasticity relates tensile stress σ and strain ε through the equation:

$$\sigma = E\varepsilon \tag{21}$$

where E is Young's modulus (stiffness) of the crust. Strictly, both the tensile stress and strain should be negative, following the convention used in the paper. However, to simplify the discussion, in this section these are taken as absolute values, in which case, as indicated above, the minus signs are not needed. The part of a rift zone that undergoes tensile strain during divergent plate movements is approximately equal to the combined width of the associated volcanic systems. If the width of the part of the rift zone that undergoes tensile strain during plate movements at a spreading rate v is denoted by u (Fig. 33), the rate of increase of tensile stress $\mathrm{d}\sigma/\mathrm{d}t$ in that part is:

$$\frac{\mathrm{d}\sigma}{\mathrm{d}t} = \frac{vE}{u} \tag{22}$$

where t is time. The reservoir is sill-like (Fig. 33) so that there is no tensile stress concentration due its shape; that is, the stress concentration factor (Figs. 16 and 17) is $k=1.0$. The time t_i for the tensile stress in the roof of the reservoir to reach the tensile strength T_0 is then:

$$t_i = \frac{T_0}{\mathrm{d}\sigma/\mathrm{d}t} = \frac{uT_0}{vE} \tag{23}$$

The units used in the equations must be homogeneous so that if, for example, the width u is in kilometres then the spreading rate v must be in kilometres (rather than millimetres) per year.

When the reservoir is not flat (sill-like) tensile stresses concentrate around it, their magnitude and location depending on the exact geometry of the reservoir, the stiffness of the host rock, as well as the loading conditions (Eqs. (6), (13–16), (19), (20)). The tensile stress concentration factor k (Figs. 16 and 17) must then be taken into account since it reduces the time between reservoir ruptures and, therefore, dyke injections. As an example, for an elongate reservoir of a shape different from that of a sill the time t_i between successive dyke injections is, from Eq. (23), given by:

$$t_i = \frac{uT_0}{vkE} \tag{24}$$

The dyke-injection frequency i_f associated with the reservoir, the reciprocal of t_i, is then:

$$i_f = \frac{1}{t_i} = \frac{vkE}{uT_0} \tag{25}$$

Eq. (25) applies to single reservoirs such as may exist beneath most of the rift-zone volcanic systems at mid-ocean ridges and elsewhere. Such reservoirs are normally the direct sources for eruptions that occur

outside composite volcanoes (Fig. 10), in which case the eruption frequency e_f is a fraction of dyke-injection frequency i_f, so that:

$$e_f = \chi i_f \tag{26}$$

where $0.0 \leq \chi \leq 1.0$. For short periods of time χ may approach 1.0. For the following reasons, however, χ is normally much less than 1.0. First, many dykes become arrested when propagating towards the surface because of various factors such as stress barriers, transverse discontinuities, and abrupt stiffness changes between layers (Gudmundsson, 2002; Gudmundsson and Brenner, 2004a,b, 2005; Gudmundsson and Philipp, 2006). Second, shallow crustal magma chambers absorb the magma in many dykes injected from the deeper reservoirs and act as dyke traps. In that case the shallow chamber and its deep source reservoir act as a double magma chamber.

7. Dyke injection from a double magma chamber

Many, and perhaps most, composite volcanoes are supplied with magma through double magma chambers. When a deep-seated magma chamber, here commonly referred to as a reservoir, acts as a source for a shallow crustal chamber the pair is referred to as a double magma chamber (Figs. 5, 10, 34). Well-known active double magma chambers in Iceland include those supplying magma to the central volcanoes of Krafla, Askja, and Grimsvötn (Fig. 3; Gudmundsson, 2000). There are reasons to believe that most, if not all, composite (central) volcanoes with collapse calderas are, or have been, fed by double magma chambers.

There is an inverse relationship between eruption frequency and eruption volume in volcanic systems in Iceland (Gudmundsson, 1998). This inverse relationship can be understood if eruptions inside composite volcanoes are fed by double magma chambers, whereas those that occur outside the composite volcanoes are fed directly from deep-seated magma reservoirs underlying the entire volcanic system (Figs. 5, 10, 34).

The shallow chamber is normally much smaller than the source reservoir, so that a single magma flow from the reservoir, lasting perhaps many years and partly received by the chamber, may trigger tens of eruptions and/or dyke injections from the chamber (Fig. 34). This volume difference is also one reason why the eruption frequency of a volcanic system is higher inside than outside its composite volcano. Another reason for the high eruption frequency of the composite volcano in comparison with the other parts of the associated volcanic system is tensile stress concentration around the shallow chamber. The resulting local stress field commonly favours the formation of a swarm of inclined sheets, with various directions and dips (Figs. 5, 10, 25, 34; Gudmundsson, 2002; Gudmundsson and Brenner, 2005; Klausen, 2004, 2006). Since the host-rock displacement is perpendicular to a sheet, the displacement across a shallow-dipping sheet close to the surface is mainly uplift. Because there are many shallow-dipping sheets in a typical sheet swarm (Fig. 25B; Gudmundsson, 2002) it follows that part of the crustal dilation associated with such a swarm is accommodated by crustal uplift rather than by horizontal crustal extension. The sheet-injection and eruption frequencies, and therefore the crustal dilation, are much higher inside than outside the composite volcano.

Mechanically, the intrusion and eruption statistics can be explained using a simplified model of a double magma chamber (Figs. 5, 10, 34). A deep-seated reservoir has a total volume V_r, with melt or magma fraction (porosity) n, pore compressibility β_p, and magma compressibility β_m. Then the total volume of magma V_r^e that flows out of the reservoir in a single magma flow is (Gudmundsson, 1987):

$$V_r^e = np_e(\beta_m + \beta_p)V_r \tag{27}$$

where p_e, the magma excess pressure in the reservoir before the magma flow starts (Eq. (1)), approaches zero

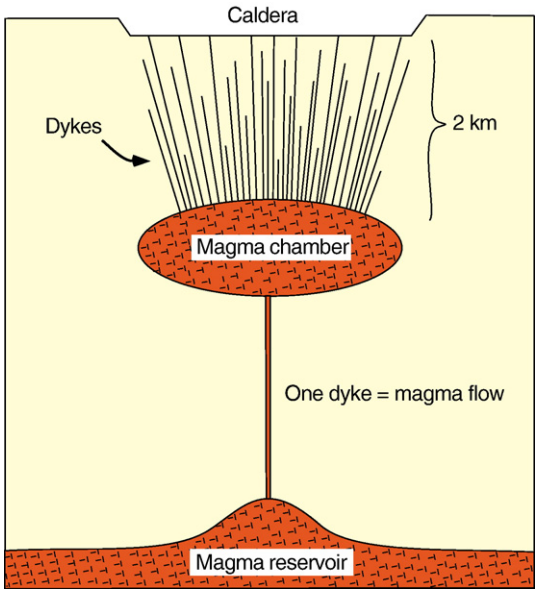

Fig. 34. Schematic, two-dimensional model of a double magma chamber. One magma flow (through a dyke) from the deep-seated, large source reservoir may trigger tens of magma flows (dykes and inclined sheets) from the smaller shallow magma chamber (cf. Fig. 25).

at the end of the flow. The corresponding equation for a crustal chamber is:

$$V_c^e = fp_e(\beta_m + \beta_c)V_c \quad (28)$$

where V_c^e is the volume of magma that flows out of a the chamber through a dyke in a single magma flow. V_c^e is approximately equal to the volume of a dyke plus, in case it is a feeder, the associated eruptive volume. The other symbols are f, the magma fraction (porosity) of the chamber, β_c, the compressibility of the rock (the upper crust) hosting the chamber, and V_c, the volume of the chamber. I use f for the magma fraction in the chamber instead of n, the symbol used for the reservoir, because the magma fraction in the chamber is normally greater than that in the reservoir.

When the shallow magma chamber is totally molten, then $f=1$ and Eq. (28) reduces to the one given by Gudmundsson (1987). Many sill-like crustal chambers at fast-spreading ridges such as the East Pacific Rise receive magma very frequently and are expected to be totally molten. By contrast, chambers at slow-spreading ridges, such as the Mid-Atlantic Ridge and parts of the rift zone in Iceland, receive magma infrequently and may be only partially molten.

The shallow chamber volume is normally less than the reservoir volume so that:

$$V_c = \lambda V_r \quad (29)$$

where $0.0 \le \lambda \le 1.0$. Consider a shallow magma chamber which receives a fraction q $(0.0 \le q \le 1.0)$ of the total magma V_r^e that flows out of a reservoir during its rupture. The tensile strength T_0 of the host rock is regarded as essentially the same for the reservoir and the shallow chamber; the excess magmatic pressure p_e in the reservoir before rupture is then the same as that in the chamber. The magma compressibility β_m is also the same for the reservoir and the chamber. By contrast, the host-rock compressibility of the chamber β_c is likely to be different from that of the reservoir β_p partly because of the much higher temperature of the rocks hosting the reservoir (Gudmundsson, 1987). Then it follows from Eqs. (27) to (29) that the number of dykes and inclined sheets N_s from the chamber triggered by a single magma flow from the reservoir is:

$$N_s = \frac{nq(\beta_m + \beta_p)}{f\lambda(\beta_m + \beta_c)} \quad (30)$$

8. Application to intrusion and eruption frequencies

Here I present several examples as to how the theoretical conclusions in the previous sections can be used to obtain quantitative results in volcanotectonics. The first example shows how to determine whether a magma chamber subject to specific loading conditions will rupture during an unrest period. The second example concerns the dyke-injection frequency at a fast-spreading ridge. The third example is on the dyke-injection and eruption frequencies of a double magma chamber in Iceland.

One basic question facing volcanologists during unrest periods is whether or not a magma chamber will rupture and inject a dyke. Stress measurements and seismic activity in a composite volcano indicate its state of stress, from which one may sometimes infer the general loading conditions to which the chamber is subject during an unrest period. While ideal geometries such as a sphere are necessarily crude approximations to the exact geometries of real chambers, ideal models can nevertheless yield results that are of great importance when assessing the probability of magma-chamber rupture, dyke injection, and associated volcanic hazards.

The regional tensile stress during a rifting episode should normally be similar to the in situ tensile strength of the crust. For common solid rocks at divergent plate boundaries, particularly for basalt, the in situ tensile strength is 0.5–6 MPa (Schultz, 1995; Amadei and Stephansson, 1997). The typical Poisson's ratio of the crust is 0.25. A spherical chamber in a rift zone may thus be expected to be subject to tensile stress that cannot exceed the maximum tensile strength (6 MPa), and would commonly be similar to the average tensile strength, of the host rock, or about 3 MPa. Substituting these values for the tensile stress and Poisson's ratio in Eqs. (13) and (14) yields $\sigma_\theta \approx -6.1$ MPa and $\sigma_\phi \approx -0.2$ MPa.

From Eq. (15) the compressive stresses at the boundary of the spherical chamber, for the given loading conditions and Poisson's ratio, is only around $\sigma_\theta \approx 1.8$ MPa. The compressive stress thus generated is far too small to cause failure of the chamber. By contrast, the tensile stress $\sigma_\theta \approx -6.1$ MPa exceeds the average tensile strength of the chamber host rock and is equal to the maximum in situ tensile strength of typical crustal rocks. It follows that, during an unrest period of this kind, magma-chamber rupture and dyke injection are to be expected at the location of the maximum tensile σ_θ.

Consider next the frequency of dyke injection into the rift zone of an ultrafast-spreading ridge with a total spreading rate of $v=17$ cm yr^{-1}. For an 8-km-wide plate-boundary zone, $u=8$ km and the static stiffness of the reservoir roof is about 70 GPa (Gudmundsson, 1990). We use the same average tensile strength as before, 3 MPa. The reservoir is assumed sill-like so that

the stress concentration factor is $k=1.0$. From Eq. (25) the long-term dyke-injection frequency i_f of the reservoir is then around 0.5 yr^{-1}. Thus, at ultrafast-spreading ridges, one dyke is injected from the associated reservoir every 2 years.

Since the shallow chambers at fast-spreading ridges are also sill-like, there is little or no stress concentration around the upper chamber, that is, $k=1.0$ (Sinton and Detrick, 1992: Mutter et al., 1995). The upper chamber appears continuous along most of the lengths of the ridge segments, and may be with melt content similar to that of the lower reservoir. Consequently, the dyke-injection frequency may be similar for the upper and lower chamber. The high dyke-injection frequency is certainly the main reason for the sheeted dyke complexes observed in depressions in the ocean floor and in ophiolites (Lippard et al., 1986; Baragar et al., 1987; Dilek et al., 1998; Karson, 1998; Stewart et al., 2003, 2005).

As a final application of the theoretical analytical results, consider the double magma chamber of the Krafla Volcano in North Iceland (Fig. 35). The width u of the zone undergoing tensile strain is here equal to the combined widths of the Holocene volcanic systems in North Iceland, about 40 km (Fig. 35). The magma reservoir underlying the Krafla Volcanic System is at a depth somewhere between 10 and 20 km (Brandsdottir et al., 1997; Gudmundsson, 2000), so that the stiffness in the roof is about 60 GPa (Gudmundsson, 1988). The total spreading rate in North Iceland is about 1.8 cm yr^{-1}; the in situ tensile strength is again taken as 3 MPa. For a source reservoir that is sill like, the dyke-injection frequency, from Eq. (25), is $i_f \approx 0.01$ yr^{-1} or one dyke injection every 100 years.

This result can now be used for the double magma chamber associated with the Krafla Volcano. The porosity of the deep-seated reservoir is $n=0.25$ and also, $f=1.0$ (Gudmundsson, 1987). The fraction of the magma volume received by the shallow chamber during flow from the reservoir is $q=0.5$, using rough estimates from Tryggvason (1984, 1986). If the volume of the shallow chamber is 0.5% of the volume of the reservoir, that is, $\lambda=0.005$, and the compressibilities of the magma and the host rock are $\beta_m=1.25\times10^{-10}$ Pa^{-1}, $\beta_p=8.8\times10^{-11}$ Pa^{-1}, and $\beta_c=2.94\times10^{-11}$ Pa^{-1} (Gudmundsson, 1987), then Eq. (30) gives the number of sheets injected by the shallow chamber during a single magma flow from the source reservoir as $N_s=34$.

These results are obviously only approximate since many of the parameters involved are poorly known. Nevertheless, the results show that a single magma flow from the magma reservoir, which lasted for 9 years during the Krafla Rifting Episode 1975–1984 (Björnsson, 1985), may have triggered 34 sheet intrusions, some of which feed eruptions, from the shallow crustal chamber of the Krafla Volcano. This conclusion fits well with data which

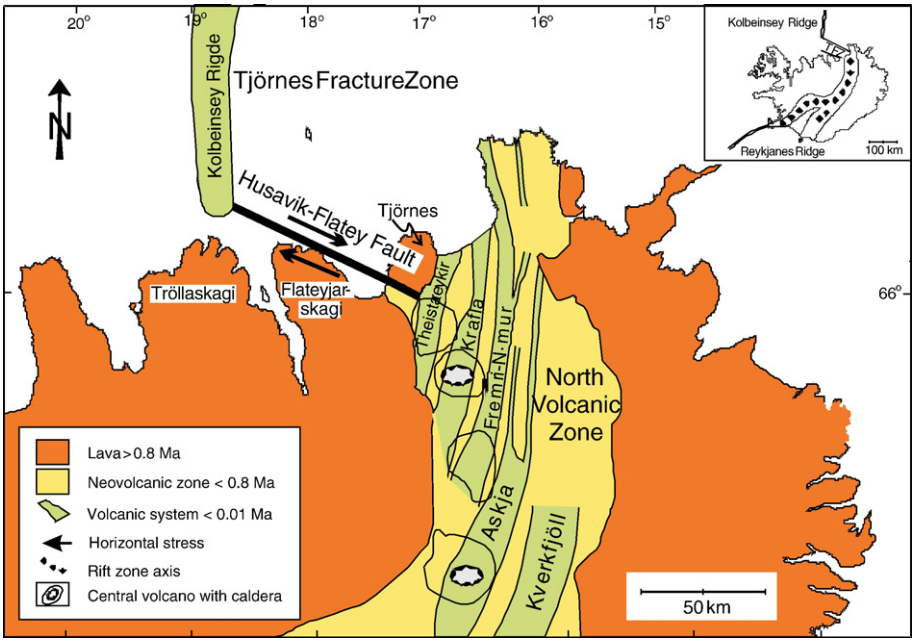

Fig. 35. Krafla Volcanic System is located, together with four other volcanic systems (green), in the North Volcanic Zone. The systems are arranged en echelon but overlap to a large extent. Each system accommodates part of the crustal dilation associated with spreading in this part of Iceland.

indicate that during the 1975–84 rifting episode the shallow chamber injected dykes at least 20–30 times, of which 9 resulted in eruptions (Björnsson, 1985; Tryggvason 1984, 1986; Harris et al., 2000).

9. Discussion

The analytical and numerical results presented in this paper underline the importance of understanding local stress fields around magma chambers and their geometries in order to evaluate volcanic hazards and, eventually, risks in active composite volcanoes and rift zones. Stress concentrations around shallow chambers, and differences in volumes between the chambers and their source reservoirs, are clearly the main reasons for the development of intense swarms of dykes and inclined sheets close to many extinct shallow magma chambers (Fig. 25). The stress concentrations and volume differences imply that local stress conditions for magma-chamber rupture and dyke injection (Eq. (1)) are normally reached much more frequently at the margin of a shallow chamber than at the margin of its source reservoir (Figs. 5, 10, 34).

The difference in intrusion frequencies between a deep reservoir and its shallow chamber is also a major reason why eruption frequencies of composite volcanoes are commonly much higher than those of the other parts of the volcanic systems (Figs. 5 and 10). Because the reservoirs are large and rupture relatively infrequently, whereas the shallow chambers are small and rupture frequently (Gudmundsson, 1998, 2000), the inverse relationship between eruption volume and eruption frequency can be explained in terms of size differences between reservoirs and chambers. Likely exceptions to this rule, however, are some fast-spreading ridges where the shallow chamber may be nearly as extensive, and of the same geometry, as the deeper reservoir (Sinton and Detrick, 1992; Mutter et al., 1995; Karson, 1998; Stewart et al., 2003, 2005). At these ridges, the dyke-injection frequencies of the shallow chamber and deep-seated reservoir may be similar.

While there is commonly an enormous number of dykes and inclined sheets in many local swarms associated with composite volcanoes and rift zones (Fig. 25; Gudmundsson, 2002; Klausen, 2004; Gudmundsson and Brenner, 2005; Klausen, 2006), there is abundant evidence that most of the sheet intrusions never reach the surface to supply magma to eruptions. That is to say, most dykes and inclined sheets become arrested in the various layers that constitute the composite volcanoes (Gudmundsson, 2002, 2003; Stewart et al., 2003; Gudmundsson and Brenner, 2004a,b, 2005; Stewart et al., 2005; Gudmundsson and Philipp, 2006). And whether they become arrested or reach the surface depends primarily on the local stresses in the layers that constitute the volcano.

The local stresses, in turn, depend on the loading conditions, including the magma-chamber geometry, and the mechanical properties of the layers of which the volcano is composed. The simplest models assume the layers hosting the magma chamber of a volcano to have the same properties everywhere (homogeneous) and identical in all directions (isotropic). Then both analytical (Figs. 13 and 18) and numerical (Figs. 19, 21, 22, 24) results show that the intensity of the local stress field associated with a chamber falls off rapidly with distance from the chamber margin. It follows that during many unrest periods when the condition for magma-chamber rupture and dyke propagation are satisfied at and in the vicinity of a chamber, the conditions for dyke arrest are satisfied at comparatively short distances from the chamber.

Models that assume the rock hosting a magma chamber to be homogeneous and isotropic are obviously oversimplifications, particularly for composite volcanoes. Nevertheless, the stress trajectories around ideal magma chambers in such crustal segments often give approximate indications of the general attitude of local swarms of inclined sheets and dykes surrounding such chambers (Fig. 25). Presumably, the main reason why such simple models match approximately the general sheet attitude is the gradual homogenisation of the mechanical properties that takes place inside the sheet swarms of composite volcanoes. As a sheet swarm evolves, the layered structure of the volcano in the vicinity of the chamber is gradually replaced by a rock unit or a shell around the chamber that consists mostly, or almost entirely, of inclined sheets and dykes (Fig. 25). Most of the (dominantly basaltic) sheets have very similar mechanical properties, so that the sheet swarm next to the chamber progressively becomes a single mechanical unit with essentially uniform properties. This development is further helped by the gradual healing and sealing of contacts through alteration and secondary mineralisation, all of which tend to bring about a unit of gradually more homogeneous and isotropic mechanical properties (Fig. 25).

Some composite volcanoes, however, do not develop dense swarms of inclined sheets. Furthermore, the near-surface parts of active composite volcanoes normally contain young lava flows and pyroclastic layers that normally have widely different mechanical properties. The local stresses in such volcanoes must be analysed using numerical models with layered host rocks. The results of the layered models (Figs. 26–32) indicate how strongly the

local stress fields of composite volcanoes can depend on the mechanical properties of the layers that constitute the volcanoes. The results also show how many composite volcanoes tend to develop local stress fields, particularly in young layers at shallow depths, that are unfavourable to feeder-dyke formation. The unfavourable local stresses develop both in horizontal layers (Figs. 26–28) and inclined (tilted) layers (Figs. 29 and 30). As a rule, layers are inclined at depth in composite volcanoes and rift zones, but inclined layers occur also at and close to the surface in many composite volcanoes (Fig. 5). The shifting of volcanic systems and zones in the down-dip direction of the lava pile, as is common in Iceland (Helgason, 1985) and at mid-ocean ridges (Stewart et al., 2005), may be partly explained in terms of the numerical models for inclined layers (Figs. 29 and 30).

The models and data presented in this paper indicate that an injected dyke reaches the surface as a feeder only if the stress field along the potential path of the dyke is favourable all the way to the surface. More specifically, the stress field along the path of an injected dyke must favour magma-fracture propagation. Since most dykes are extension (mode I) fractures (Gudmundsson, 2002), this means that the stress field must encourage extension-fracture formation along the entire path of the dyke for it to become a feeder. For this to be possible, all the local stresses in all the layers that the feeder-dyke dissects on its way to the surface (Figs. 4 and 28) must be essentially the same. This means that the stress field along this path must be homogenised.

Homogenisation of the local stresses in a composite volcano presumably occurs primarily through two mechanisms. One is host-rock alteration, the other host-rock deformation. During alteration, there is healing and sealing of contacts and faults and filling of fractures and cavities in the rock with secondary minerals. Consequently, the thicknesses of rock units with essentially the same (homogeneous) mechanical properties gradually increase. The main processes involved in host-rock deformation of composite volcanoes are the injection of dykes and inclined sheets and faulting. At shallow depths in active composite volcanoes and rift zones, normal faulting may dominate, but dyke and sheet injection at greater depths (Gudmundsson, 2000, 2002; Acocella and Neri, 2003; Walter et al., 2005). Both dyke injection and normal faulting tend to smooth out the stress differences between layers and make the stress fields basically homogeneous in large parts of the composite volcano.

10. Conclusions

One principal aim of volcanology is to provide a theoretical understanding of the mechanical processes that occur inside composite volcanoes during unrest periods. Here I have argued that many of these processes, particularly faulting, surface deformation, dyke emplacement and, eventually, magma transport to the surface depend strongly on the local stresses in the layers that constitute the volcano. Furthermore, I argue that if the local stresses within a volcano can be determined one should in principle be able to infer whether dykes injected from a chamber, or faults propagating at depth in a volcano such as during collapse-caldera formation, are likely to reach the surface.

Currently available technology makes it difficult to determine accurately local stresses in composite volcanoes. However, the infrastructures of many composite volcanoes, active and inactive, can be obtained through geological and geophysical studies of deeply eroded, well-exposed sections and drill cores. The distribution of earthquakes in an active volcano is also an indication of its local stress fields. For example, if the earthquakes generated during an unrest period with magma-chamber inflation are essentially evenly distributed within the volcano the local stress fields are likely to be similar throughout the volcano. The stress field may then be regarded as comparatively homogeneous and, when favouring vertical extension fractures, likely to encourage injected dykes to propagate to the surface, resulting in eruptions.

By contrast, the earthquakes during an unrest period may be mostly confined to certain rock bodies or mechanical layers within the volcano. Then the local stress fields are likely to be dissimilar, that is, the stress field in one mechanical layer is very different from the stress fields in the adjacent layers. The general state of stress in the volcano may then be regarded as comparatively heterogeneous and likely to prevent volcanic eruptions.

To know the state of stress in a volcano is therefore very important when attempting to answer the most important question facing earth scientists and civil authorities during a volcanic unrest period: namely, is an eruption likely to occur? The analytical and, in particular, the numerical models presented in this paper should help to assess the likely local stress fields in volcanoes with various magma-chamber geometries, and in different tectonic regimes. These and other similar models can thus be valuable tools when estimating hazards and risks during unrest periods. To refine the models and to make them more useful in hazard studies, however, we need to be able to test them. And one, and perhaps the best, way to check the models' test implications is through direct stress measurements in volcanoes.

In conclusion, what is clearly needed to improve our understanding of unrest periods and our assessment of

volcanic hazards and risks is stress monitoring of active volcanoes. Stress monitoring through seismicity and crustal deformation is important but gives only general indications of the state of stress. Real stress monitoring of selected composite volcanoes can only be achieved by using in situ stress measurements in many of the mechanical layers that constitute the volcano and comparing the results with numerical-model predictions and field observations.

Acknowledgements

I thank Isabel Bivour, Steffi Burchardt, Gabriele Ertl, Nadine Friese, and Sonja Philipp for running some of the numerical models and for help with the figures. I also thank the reviewers, Valerio Acocella and Joan Marti, for very helpful comments. Part of the work reported here was supported by grants from the Research Council of Norway, the Geological Survey of Norway (NGU), Norsk Hydro, Statoil, and the European Commission through the project Prepared (EVG1-CT-2002-00073).

References

Acocella, V., Neri, M., 2003. What makes flank eruptions? The 2001 Etna eruption and its possible triggering mechanisms. Bull. Volcanol. 65, 517–529.

Acocella, V., Korme, T., Salvini, F., Funiciello, R., 2003. Elliptic calderas in the Ethiopian Rift: control of pre-existing structures. J. Volcanol. Geotherm. Res. 119, 189–203.

Acocella, V., Porreca, M., Neri, M., Massimi, E., Mattei, M., 2006a. Propagation of dikes at Vesuvio (Italy) and the effect of Mt. Somma. Geophys. Res. Lett. 33 (Art. No. L08301, April 18, 2006).

Acocella, V., Porreca, M., Neri, M., Mattei, M., Funiciello, R., 2006b. Fissure eruptions at Mount Vesuvius (Italy): insights on the shallow propagation of dikes at volcanoes. Geology 34, 637–676.

Afrouz, A.A., 1992. Practical Handbook of Rock Mass Classification Systems and Modes of Ground Failure. CRC Press, London.

Amadei, B., Stephansson, O., 1997. Rock Stress and its Measurement. Chapman and Hall, London.

Anderson, E.M., 1936. The dynamics of formation of cone sheets, ring dykes and cauldron subsidences. Proc. R. Soc. Edinb. 56, 128–163.

Baragar, W.R.A., Lambert, M.B., Baglow, N., Gibson, I.L., 1987. Sheeted dykes of the Troodos ophiolite, Cyprus. In: Halls, H.C., Fahrig, W.F. (Eds.), Mafic Dyke Swarms Geol. Assoc. Canada Spec. Pap., vol. 34, pp. 257–272.

Battaglia, M., Segall, P., Murray, J., et al., 2003. The mechanics of unrest at Long Valley caldera, California: 1. Modeling the geometry of the source using GPS, leveling and two-color EDM data. J. Volcanol. Geotherm. Res. 127, 195–217.

Bell, F.G., 2000. Engineering Properties of Soils and Rocks, 4th ed. Blackwell, Oxford.

Benham, P.P., Crawford, R.J., Armstrong, C.G., 1996. Mechanics of Engineering Materials, 2nd ed. Prentice Hall, New Jersey.

Beswick, A.E., 1965. A Study of the Slaufrudalur Granophyre Intrusion, South-East Iceland. PhD Thesis, Imperial College, London.

Björnsson, A., 1985. Dynamics of crustal rifting in NE Iceland. J. Geophys. Res. 90, 10,151–10,162.

Bonafede, M., Rivalta, E., 1999. The tensile dislocation problem in a layered elastic medium. Geophys. J. Int. 136, 341–356.

Bonafede, M., Dragoni, M., Quareni, F., 1986. Displacement and stresss fields produced by a centre of dilation and by a pressure source in a viscoelastic half-space: application to the study of ground deformation and seismic activity at Campi Flegrei, Italy. Geophys. J. R. Astron. Soc. 87, 455–485.

Boresi, A.P., Sidebottom, O.M., 1985. Advanced Mechanics of Materials, 4th ed. Wiley, New York.

Brandsdottir, B., Menke, W., Einarsson, P., White, R.S., Staples, R.K., 1997. Faroe-Iceland ridge experiment 2. Crustal structure of the Krafla central volcano. J. Geophys. Res. 102, 7867–7886.

Brebbia, C.A., Dominquez, J., 1992. Boundary Elements: An Introductory Course. Computational Mechanics, Boston.

Calvari, S., Neri, M., Pinkerton, H., 2003. Effusion rate estimations during the 1999 summit eruption on Mount Etna, and growth of two distinct lava flow fields. J. Volcanol. Geotherm. Res. 119, 107–123.

Cargill, H.K., Hawkes, L., Ledeboer, J.A., 1928. The major intrusions of south-eastern Iceland. Q. J. Geol. Soc. Lond. 84, 505–539.

Carmichael, R.S., 1989. Practical Handbook of Physical Properties of Rocks and Minerals. CRC Press, London.

Cas, R., Wright, J., 1987. Volcanic Successions: Modern and Ancient. Kluwer, New York.

Chester, D., 1993. Volcanoes and Society. Edward Arnold, London.

Daniel, I.M., Ishai, O., 1994. Engineering Mechanics of Composite Materials. Oxford University Press, Oxford.

Davis, P.M., 1986. Surface deformation due to inflation of an arbitrarily oriented triaxial ellipsoidal cavity in an elastic half space, with reference to Kilauea volcano, Hawaii. J. Geophys. Res. 91, 7429–7438.

Delaney, P.T., McTigue, D.F., 1994. Volume of magma accumulation or withdrawal estimated from surface uplift or subsidence, with application to the 1960 collapse of Kilauea Volcano. Bull. Volcanol. 56, 417–424.

De Natale, G., Pingue, F., 1993. Ground deformation in collapsed calderas structures. J. Volcanol. Geotherm. Res. 57, 19–38.

Dilek, Y., Moores, E.M., Furnes, H., 1998. Structure of modern oceanic crust and ophiolites and implications for faulting and magmatism at oceanic spreading centers. In: Buck, W.R., Delaney, P.T., Karson, J.A., Lagabrielle, Y. (Eds.), Faulting and Magmatism at Mid-Ocean Ridges. AGU, Washington, pp. 219–265.

Egilsson, D., Hardarson, B.A., Jonsson, B., 1989. Dynamic properties of rock. Yearbook of the Engng. Assoc. Iceland, pp. 226–233 (in Icelandic).

Ernst, R.E., Grosfils, E.B., Mege, D., 2001. Giant dike swarms: Earth, Venus, and Mars. Annu. Rev. Earth Planet. Sci. 29, 489–534.

Eshelby, J.D., 1957. The determination of the elastic field of an ellipsoidal inclusion, and related problems. Proc. R. Soc. Lond., A 241, 376–396.

Farmer, I., 1983. Engineering Behaviour of Rocks, 2nd ed. Chapman and Hall, London.

Fialko, Y.A., Rubin, A.M., 1999. Thermal and mechanical aspects of magma emplacement in giant dike swarms. J. Geophys. Res. 104, 23033–23049.

Fisher, R.V., Schmincke, H.U., 1984. Pyroclastic Rocks. Springer, Berlin.

Folch, A., Marti, J., 1998. The generation of overpressure in felsic magma chambers. Earth Planet. Sci. Lett. 163, 301–314.

Folch, A., Fernandez, J., Rundle, J.B., Marti, J., 2000. Ground deformation in a viscoelastic medium composed of a layer

overlying a half-space: a comparison between point and extended sources. Geophys. J. Int. 140, 37–50.
Fridleifsson, G.O., 1993. The Geology and the Alteration History of the Geitafell Central Volcano, Southeast Iceland. PhD Thesis, University of Edinburgh, Edinburgh.
Freundt, A., Rosi, M. (Eds.), 2001. From Magma to Tephra: Modelling Physical Processes of Explosive Volcanic Eruptions. Elsevier, New York.
Goodier, J.N., 1933. Concentration of stress around spherical inclusions and flaws. Trans. Am. Soc. Mech. Eng. 55, 39–44.
Gudmundsson, A., 1987. Formation and mechanics of magma reservoirs in Iceland. Geophys. J. R. Astron. Soc. Lond. 91, 27–41.
Gudmundsson, A., 1988. Effect of tensile stress concentration around magma chambers on intrusion and extrusion frequencies. J. Volcanol. Geotherm. Res. 35, 179–194.
Gudmundsson, A., 1990. Emplacement of dikes, sills and crustal magma chambers at divergent plate boundaries. Tectonophysics 176, 257–275.
Gudmundsson, A., 1998. Magma chambers modeled as cavities explain the formation of rift zone central volcanoes and their eruption and intrusion statistics. J. Geophys. Res. 103, 7401–7412.
Gudmundsson, A., 2000. Dynamics of volcanic systems in Iceland: example of tectonism and volcanism at juxtaposed hot spot and mid-ocean ridge system. Annu. Rev. Earth Planet. Sci. 28, 107–140.
Gudmundsson, A., 2002. Emplacement and arrest of sheets and dykes in central volcanoes. J. Volcanol. Geotherm. Res. 116, 279–298.
Gudmundsson, A., 2003. Surface stresses associated with arrested dykes in rift zones. Bull. Volcanol. 65, 606–619.
Gudmundsson, A., Brenner, S.L., 2004a. How mechanical layering affects local stresses, unrests, and eruptions of volcanoes. Geophys. Res. Lett. 31. doi:10.1029/2004GL020083.
Gudmundsson, A., Brenner, S.L., 2004b. Local stresses, dyke arrest and surface deformation in volcanic edifices and rift zones. Annals Geophys. 47, 1433–1454.
Gudmundsson, A., Brenner, S.L., 2005. On the conditions of sheet injections and eruptions in stratovolcanoes. Bull. Volcanol. 67, 768–782.
Gudmundsson, A., Philipp, S.L., 2006. How local stress fields prevent volcanic eruptions. J. Volcanol. Geotherm. Res. doi:10.1016/j.jvolgeores.2006.06.005.
Haimson, B.C., Rummel, F., 1982. Hydrofracturing stress measurements in the Iceland research drilling project drill hole at Reydarfjordur, Iceland. J. Geophys. Res. 87, 6631–6649.
Harris, A.J.L., Murray, J.B., Aries, S.E., Davies, M.A., Flynn, L.P., Wooster, M.J., Wright, R., Rothery, D.A., 2000. Effusion rate trends at Etna and Krafla and their implications for eruptive mechanisms. J. Volcanol. Geotherm. Res. 102, 237–270.
Helgason, J., 1985. Shifts of the plate boundary in Iceland — some aspects of Tertiary volcanism. J. Geophys. Res. 90, 84–92.
Holohan, E.P., Troll, V.R., Walter, T.R., Munn, S., McDonnell, S., Shipton, Z.K., 2005. Elliptical calderas in active tectonic settings: an experimental approach. J. Volcanol. Geotherm. Res. 144, 119–136.
Hudson, J.A., Harrison, J.P., 1997. Engineering Rock Mechanics: An Introduction to the Principles. Pergamon, Oxford.
Hyer, M.W., 1998. Stress Analysis of Fiber-Reinforced Composite Materials. McGraw-Hill, New York.
Jeffrey, G.B., 1921. Plane stress and plane strain in bipolar coordinates. Philos. Trans. R. Soc. Lond., A 221, 265–293.
Jing, L., Hudson, J.A., 2002. Numerical models in rock mechanics. Int. J. Rock Mech. Min. Sci. 39, 409–427.
Jonsson, B., 1971. Geotechnical Properties of Tillite and Moberg from Southern Central Iceland. MSc. Thesis, University of Durham, Durham.
Karson, J.A., 1998. Internal structure of the oceanic lithosphere: a perspective from tectonic windows. In: Buck, W.R., Delaney, P.T., Karson, J.A., Lagabrielle, Y. (Eds.), Faulting and Magmatism at Mid-Ocean Ridges. AGU, Washington, pp. 177–218.
Kaw, A.K., 1997. Mechanics of Composite Materials. CRC Press, London.
Keer, L.M., Xu, Y., Luk, V.K., 1998. Boundary effects in penetration or perforation. J. Appl. Mech. 65, 489–496.
Kilburn, C.R.J, Lopes, R.M.C., 1991. General patterns of flow field growth — aa and blocky lavas. J. Geophys. Res. 96, 19721–19732.
Klausen, M.B., 2004. Geometry and mode of emplacement of the Thverartindur cone sheet swarm, SE Iceland. J. Volcanol. Geotherm. Res. 138, 185–204.
Klausen, M.B., 2006. Geometry and mode of emplacement of dike swarms around the Birnudalstindur igneous centre, SE Iceland. J. Volcanol. Geotherm. Res. 151, 340–356.
Klugel, A., Walter, T.R., Schwarz, S., Geldmacher, J., 2005. Gravitational spreading causes en-echelon diking along a rift zone of Madeira Archipelago: an experimental approach and implications for magma transport. Bull. Volcanol. 68, 37–46.
Lekhnitskii, S.G., 1968. Anisotropic Plates. Gordon and Breach, New York.
Lippard, S.J., Shelton, A.W., Gass, I. (Eds.), 1986. The Ophiolite of Northern Oman. Blackwell, Oxford.
Lister, J.R., Kerr, R.C., 1991. Fluid-mechanical models of crack propagation and their application to magma transport in dykes. J. Geophys. Res. 96, 10,049–10,077.
Logan, D.L., 2002. A First Course in the Finite Element Method. Brooks/Cole, Pacific Grove, USA.
Love, A.E.H., 1927. A Treatise on the Mathematical Theory of Elasticity. Dover, New York.
Lungarini, L., Troise, C., Meo, M., DeNatale, G., 2005. Finite element modelling of topographic effects on elastic ground deformation at Mt. Etna. J. Volcanol. Geotherm. Res. 144, 257–271.
Marsh, B.D., 1989. Magma chambers. Annu. Rev. Earth Planet. Sci. 17, 439–474.
Maugis, D., 2000. Contact, Adhesion and Rupture of Elastic Solids. Springer, Berlin.
McTigue, D.F., 1987. Elastic stress and deformation near a finite spherical magma body: resolution of the point source paradox. J. Geophys. Res. 92, 12,931–12,940.
Mege, D., Korme, T., 2004. Dyke swarm emplacement in the Ethiopian large igneous province: not only a matter of stress. J. Volcanol. Geotherm. Res. 132, 283–310.
Melan, E., 1932. Point force at internal point in a semi-infinite plate. Z. Angew. Math. Mech. 12, 343–346 (in German).
Mindlin, R.D., 1936. Force at a point in the interior of a semi-infinite solid. Physics 7, 195–202.
Mogi, K., 1958. Relations between eruptions of various volcanoes and the deformations of the ground surfaces around them. Bull. Earthq. Res. Inst. Univ. Tokyo 36, 99–134.
Mutter, J.C., Carbotte, S.M., Su, W.S., Xu, L.Q., Buhl, P., Detrick, R.S., Kent, G.M., Orcutt, J.A., Harding, A.J., 1995. Seismic images of active magma systems beneath the East Pacific Rise between 17-Degrees-05′ and 17-Degrees-35's. Science 268, 391–395.
Myrvang, A., 2001. Rock Mechanics. Norway University of Technology (NTNU), Trondheim (in Norwegian).
Nemat-Nasser, S., Hori, M., 1999. Micromechanics: Overall Properties of Heterogeneous Materials, 2nd ed. Elsevier, Amsterdam.

Newhall, C.G., Dzurisin, D., 1988. Historical Unrest of Large Calderas of the World. U.S. Geological Survey Bulletin, vol. 1855. Reston, VA.
Oddson, B., 1984. Geology and Geotechnical Behaviour of the Young Volcanic Rocks of Iceland with Emphasis on the Effects of Petrography. PhD Thesis, ETH, Zürich (in German).
Pinel, V., Jaupart, C., 2000. The effect of edifice load on magma ascent beneath a volcano. Philos. Trans. R. Soc. Lond., A 358, 1515–1532.
Pinel, V., Jaupart, C., 2003. Magma chamber behavior beneath a volcanic edifice. J. Geophys. Res. 108 (Art. 2072, February 4).
Pinel, V., Jaupart, C., 2004. Magma storage and horizontal dyke injection beneath a volcanic edifice. Earth Planet. Sci. Lett. 221, 245–262.
Pollard, D.D., Delaney, P.T., Duffield, W.A., Endo, E.T., Okamura, A.T., 1983. Surface deformation in volcanic rift zones. Tectonophysics 94, 541–584.
Priest, S.D., 1993. Discontinuity Analysis for Rock Engineering. Chapman and Hall, London.
Rivalta, E., Bottiner, M., Dahm, T., 2005. Buoyancy-driven fracture ascent: experiments in layered gelatine. J. Volcanol. Geotherm. Res. 144, 273–285.
Rossi, M.J., 1996. Morphology and mechanism of eruption of postglacial shield volcanoes in Iceland. Bull. Volcanol. 57, 530–540.
Rubin, A.M., 1995. Propagation of magma-filled cracks. Annu. Rev. Earth Planet. Sci. 23, 287–336.
Saada, A.S., 1983. Elasticity: Theory and Applications. Krieger, Malabar, Florida.
Sadd, M.H., 2005. Elasticity: Theory, Applications, and Numerics. Elsevier, Amsterdam.
Sadowsky, M.A., Sternberg, E., 1947. Stress concentration around an ellipsoidal cavity in an infinite body under arbitrary plane stress perpendicular to the axis of revolution of cavity. J. Appl. Mech. 14, A191–A201.
Sadowsky, M.A., Sternberg, E., 1949. Stress concentration around a triaxial ellipsoidal cavity. J. Appl. Mech. 16, 149–157.
Saemundsson, K., 1978. Fissure swarms and central volcanoes of the neovolcanic zones of Iceland. In: Bowes, D.R., Leake, B.E. (Eds.), Crustal Evolution in Northwestern Britain and Adjacent Regions-Geol. J. Spec. Issue No. 10, pp. 415–432.
Sanford, R.J., 2003. Principles of Fracture Mechanics. Prentice-Hall, New Jersey.
Savin, G.N., 1961. Stress Concentration Around Holes. Pergamon, New York.
Schmincke, H.U., 2004. Volcanism. Springer, Berlin.
Schön, J.H., 2004. Physical Properties of Rocks: Fundamentals and Principles of Petrophysics. Elsevier, Oxford.
Schultz, R.A., 1995. Limits on strength and deformation properties of jointed basaltic rock masses. Rock Mech. Rock Eng. 28, 1–15.
Self, S., Thordarson, T., Keszthelyi, L., Walker, G.P.L., Hon, K., Murphy, M.T., Long, P., Finnemore, S., 1996. A new model for the emplacement of Columbia River Basalts as large, inflated pahoehoe lava flow fields. Geophys. Res. Lett. 23, 2689–2692.
Sibett, B.S., 1988. Size, depth and related structures of intrusions under stratovolcanoes and associated geothermal systems. Earth Sci. Rev. 25, 291–309.
Sinton, J.M., Detrick, R.S., 1992. Mid-ocean magma chambers. J. Geophys. Res. 97, 197–216.
Soutas-Little, R.W., 1973. Elasticity. Dover, New York.
Sparks, R.S.J., Bursik, M.I., Carey, S.N., Gilbert, J.S., Glaze, L.S., Sigurdsson, H., 1997. Volcanic Plumes. Wiley, New York.
Stewart, M.A., Klein, E.M., Karson, J.A., Brophy, J.G., 2003. Geochemical relationships between dikes and lavas at the Hess Deep Rift: implications for magma eruptibility. J. Geophys. Res. 108. doi:10.1029/2001JB001622 (Art. 2184).
Stewart, M.A., Karson, J.A., Klein, M.A., 2005. Four-dimensional upper crustal construction at fast-spreading mid-ocean ridges: a perspective from an upper crustal cross-section at the Hess Deep Rift. J. Volcanol. Geotherm. Res. 144, 287–309.
Tan, S.C., 1994. Stress Concentrations in Laminated Composites. Technomic, Basel.
Timoshenko, S., Goodier, J.N., 1970. Theory of Elasticity, 3rd ed. McGraw-Hill, New York.
Torfason, H., 1979. Investigations into the Structure of South-Eastern Iceland, PhD Thesis, University of Liverpool, Liverpool.
Trasatti, E., Giunchi, C., Bonafede, M., 2005. Structural and rheological constraints on source depth and overpressure estimates at Campi Flegrei caldera. Italy. J. Volcanol. Geotherm. Res. 144, 105–118.
Tryggvason, E., 1984. Widening of the Krafla fissure swarm during the 1975–1981 volcano-tectonic episode. Bull. Volcanol. 47, 47–69.
Tryggvason, E., 1986. Multiple magma reservoirs in a rift zone volcano: ground deformation and magma transport during the September 1984 eruption of Krafla, Iceland. J. Volcanol. Geotherm. Res. 28, 1–44.
Tsuchida, E., Nakahara, I., 1970. Three-dimensional stress concentration around a spherical cavity in a semi-infinite elastic body. Jpn. Soc. Mech. Eng., Bull. 13, 499–508.
Walker, G.P.L., 1963. The Breiddalur Central Volcano, eastern Iceland. Q. J. Geol. Soc. Lond. 119, 29–63.
Walker, G.P.L., 1991. Structure, and origin by injection of lava under surface crust, of tumuli, lava rises, lava-rise pits, and lava-inflation clefts in Hawaii. Bull. Volcanol. 53, 546–558.
Walter, T.R., Acocella, V., Neri, M., Amelung, F., 2005. Feedback processes between magmatic events and flank movement at Mount Etna (Italy) during the 2002–2003 eruption. J. Geophys. Res. 110 (B10) (Art. No. 10205, October 27, 2005).
Zienkiewicz, O.C., 1977. The Finite Element Method. McGraw-Hill, New York.